

Recombination and Metastability in Amorphous Silicon and Silicon- Germanium Alloys

Final Subcontract Report
1 February 1991 – 31 January 1994

M. Silver, D. X. Han, K. D. Wang,
M. Kemp
*University of North Carolina
Chapel Hill, North Carolina*

NREL technical monitor: H. M. Branz



MASTER

National Renewable Energy Laboratory
1617 Cole Boulevard
Golden, Colorado 80401-3393
A national laboratory of the U.S. Department of Energy
Managed by Midwest Research Institute
for the U.S. Department of Energy
under contract No. DE-AC02-83CH10093

Prepared under Subcontract No. XG-1-10063-5

July 1994

NOTICE

NOTICE: This report was prepared as an account of work sponsored by an agency of the United States government. Neither the United States government nor any agency thereof, nor any of their employees, makes any warranty, express or implied, or assumes any legal liability or responsibility for the accuracy, completeness, or usefulness of any information, apparatus, product, or process disclosed, or represents that its use would not infringe privately owned rights. Reference herein to any specific commercial product, process, or service by trade name, trademark, manufacturer, or otherwise does not necessarily constitute or imply its endorsement, recommendation, or favoring by the United States government or any agency thereof. The views and opinions of authors expressed herein do not necessarily state or reflect those of the United States government or any agency thereof.

Printed in the United States of America

Available to DOE and DOE contractors from:
Office of Scientific and Technical Information (OSTI)
P.O. Box 62
Oak Ridge, TN 37831
Prices available by calling (615) 576-8401

Available to the public from:
National Technical Information Services (NTIS)
U.S. Department of Commerce
5285 Port Royal Road
Springfield, VA 22161
(703) 487-4650



DISCLAIMER

Portions of this document may be illegible electronic image products. Images are produced from the best available original document.

PREFACE

The work was under subcontract No XG-1-10063-5 during the time period of February 1, 1991 - January 31, 1994. The work at Chapel Hill was performed by

Professor Marvin Silver

Dr. Daxing Han - Research Associate Professor

Dr. Keda Wang - Research Associate

Dr. Mathieu Kemp - Research Associate

The principal investigator, Dr. Silver died during the course of the work and Dr. Han subsequently became the principal investigator.

Over last 3 years, we studied the p-i-n samples obtained through collaboration with Solarex, the Institute for Energy Conversion (IEC), Chronar, Advanced Photovoltaic Systems (APS), and the National Renewable Energy Laboratory (NREL). Our research has resulted in the publications of 19 papers (see references) and the submission of three annual reports.

SUMMARY

We have studied electroluminescence (EL), transient current, and photocurrent before and after light-soaking in a-Si:H p-i-n device structures. We perfected the EL measurement techniques for a-Si:H p-i-n solar cells, which include EL spectral, EL transient, and their temperature dependence. In order to find where the recombination takes place and what states are involved in photodegradation processes, we focused on EL and transient forward bias current as a function of device parameters such as thickness of the i-layer and p-i junction properties before and after photodegradation.

In section A of the report we give the results of EL measurements, with particular reference to the effect of the buffer layer on EL spectra and how the EL spectral line shape changes with the i-layer thickness. We have found that in thin cells with buffered layers, p-b-i-n structures, the main-band luminescence was more pronounced than in simple p-i-n structures. We also found that, at elevated temperatures, thin p-i-n devices displayed primarily defect luminescence (0.8-0.9 eV) while, for thick p-i-n ($\geq 2 \mu\text{m}$), the luminescence observed was the main-band domination (1.1-1.2 eV). For the first time, we were able to distinguish between bulk- and junction-controlled recombination. We conclude that the quality of the p-i interface is very important in solar cell performance.

Generally there is a decrease of the main-band luminescence but an increase of the defect-band luminescence after light-soaking. However, when the "main-band" is more pronounced, either in the p-b-i-n sample or at higher applied V, the photodegradation of this band is more obvious. So it is reasonable to surmise that the Staebler-Wronski effect is due to the high-energy (1.2 eV) recombination, and it is not directly related to defect-controlled recombination. In thin samples ($\leq 0.5 \mu\text{m}$), defects dominate the recombination, so the Staebler-Wronski effect is either smaller or slower because only a very small fraction of the recombination involves the band tails.

As described in section B, in order to study the light-soaking effects on deep-trapping and recombination processes in p-i-n cells, transient current measurements before and after light-soaking were made. Surprisingly, the current rise time after light-soaking delayed more than one order of magnitude, but the final current did not change much. In other words, the response time was more than 10 times longer at light-soaked state B but the steady-state $\mu\tau$ product did not change much. So there must be a new mechanism rather than the standard picture of gap states to give this long delay time. Defect-relaxation concept is suggested to explain the slow response in light-soaked state B. Slow relaxation was also observed in optical bias measurements in a-Si:H films. So we conclude that the slow relaxation is a bulk effect.

To study whether the charges are stored near the junction or in the bulk, we measured the thickness dependence of forward bias current as a function of repetition rate and reverse bias between forward bias pulses. Few repetition rate and reverse bias effects were found in thin ($0.4 \mu\text{m}$) p-i-n samples when compared with thick ones ($\geq 2.0 \mu\text{m}$), implying that the junctions recover faster than the bulk when subjected to excess carriers due to bias.

In section C of the report, we give photocurrent results obtained in collaboration with R. Vanderhagen in France. The forward photocurrent is much larger than the reverse photocurrent, indicating a large gain on the order of 100-1,000 for the $2.0\text{-}\mu\text{m}$ -thick n-i-p samples. This implies that, in those samples, the lifetime is longer than the transit time.

The theoretical work is discussed in section D. By including the coulomb interaction, we made progress on a microscopic model for radiative recombination. These calculations reproduce the frequency spectra of low temperature luminescence.

Table of Contents

Notice	ii
Preface	iii
Summary	iv
Table of Contents	v
List of Figures	vi
INTRODUCTION	1
RESULTS	2
A. Electroluminescence in a-Si:H p-i-n cells.	2
1. Buffer-Layer Dependence of EL Spectra	2
2. i-layer Thickness Dependence of EL Spectra	4
3. Applied Voltage Dependence of EL Spectra	6
4. EL Decay and Recombination Lifetime Distribution	7
5. Light-Soaking Effect on EL Spectra.....	9
6. Light-Soaking Effect on EL Decay	11
7. Conclusions.....	13
B. Light-Soaking Effect on Transient Current in a-Si:H p-i-n cells	14
1 Repetition Rate Dependence of Transient Forward Bias Current in p-i-n cells	14
2. Reverse Bias Effects on Transient Forward Current in p-i-n	16
3. Slow Relaxation Processes in a-Si:H	18
4. Conclusions.....	19
C. Light-soaking Effect on Photo-Gain in a-Si:H n-i-p cells	20
1. Experimental results	20
2. Conclusions.....	22
D. Theoretical Results	23
1. A Simple Model of Recombination Current and EL in a-Si:H	23
2. An Explanation for the Shape of the Forward Bias Current..	24
3. A Microscopic Model for Radiative Recombination.	25
4. H-Diffusion Including Deep Trap Levels	26
REFERENCES	28

List of Figures

- Fig. 1 Comparison of the EL spectra between 0.4- μm buffered and non-buffered solar cells made by Solarex. The curves with open circles and crosses correspond to p-i-n and p-b-i-n, respectively. (a) Data measured at 300 K and (b) 200 K.
- Fig. 2 Comparison of the EL spectra between 0.5- μm buffered and non-buffered solar cells made by IEC. EL spectra measured under 0.9 V at 300 K. The upper and lower curves correspond to p-b-i-n and p-i-n, respectively.
- Fig. 3 Thickness dependence of EL spectra in p-i-n structures. The i-layer thickness was 0.2, 0.4, 2.0, and 10.0 μm . (a) At 300 K, and (b) 200 K.
- Fig. 4 Applied voltage dependence of EL spectra at 300 K. (a) In a 0.2- μm p-i-n, and (b) in a 2.0- μm p-i-n.
- Fig. 5 Temperature dependence of EL recombination lifetime distribution in a 2.0- μm p-i-n at temperatures of 120, 150, 180, 230, and 300 K.
- Fig. 6 The peak positions of fast and slow lifetime vs. $1/T$. Data from the same sample as in Fig. 5.
- Fig. 7 Photodegradation on EL spectra in 0.5- μm solar cells at 300 K under low and high applied voltage. (a) under 0.8 V, and (b) 3 V.
- Fig. 8 Light-soaking effect on EL spectra in a 2.0- μm p-i-n, under 4 V, at 300K.
- Fig. 9 Photodegradation effect on transient EL decay in a 0.4 μm p-i-n after a 4-V pulse at 100 K. (a) Total EL signal decay at state A and state B, (b) the lifetime distribution at state A and state B, and data deduced from Fig. 9a.
- Fig. 10 Pulse repetition rate dependence of transient forward bias current $I(t)$ in a 10- μm thick p-i-n. (a) In state A, and (b) state B.
- Fig. 11 Pulse repetition rate dependence of transient forward current $I(t)$ in a 0.4- μm p-i-n at 300 K.
- Fig. 12 Negative bias effect on transient forward bias current in a 10- μm p-i-n diode at 300 K. (a) In state A, and (b) state B.
- Fig. 13 Negative bias effect on transient forward bias current in a 0.4- μm p-i-n diode at 300 K in state A.
- Fig. 14 Forward current decay in a 2- μm p-i-n diode at 300 K. The data were taken by 3 V/0 V/3 V and 5 V/0 V/5 V pulses.
- Fig. 15 The transient photocharge $Q(t)/(d^2/Q_0V)$ recorded at four optical bias levels and in the dark in an a-Si:H specimen in a light-soaked state. The dc currents through the specimen were 2.7×10^{-7} A, 1.8×10^{-8} A, 1.0×10^{-9} A, 4.8×10^{-10} A, and 5.0×10^{-11} A, from the top to the bottom curves.
- Fig. 16 Forward bias dark and photocurrent vs. $V_a - V_{bi}$ for a 1- μm n-i-p diode before and after light degradation. Squares and triangles indicate before and after degradation.

- Fig. 17 Forward photocurrent vs. photo-flux in 1- μm n-i-p. Triangles and squares correspond to undegraded and light-degraded states. The voltage across the i-layer is indicated. The dark current is indicated with arrows.
- Fig. 18 Photo-gain as a function of red light degradation time (AM10 equivalent). Open circles pertain to a sample that has been partially annealed (140°C) and degraded again.
- Fig. 19 Schematic plot of the current flow through a p-i-n diode.
- Fig. 20 Distribution of potential fluctuation v due to a dilute density of charges.
- Fig. 21 D diffusion profile for four different times after the onset of diffusion. Position, x , is scaled by the mean atomic displacement between trapping events λ . Time, t , is scaled by the detrapping time τ . Tracer concentration, θ , is scaled by the initial tracer density θ_0 .
- Table I Sample Preparation Conditions and Cell Performance.

INTRODUCTION

Our goal is to understand (1) how recombination, trapping, and band-mobility modification affecting the electronic properties of amorphous semiconductors can be measured, characterized, and described by an appropriate spectrum of defect states and (2) how light-induced defects in a-Si:H and native defects in a-SiGe:H affect transport properties in these materials.

It is well-known that light-induced effects (SWE) increase the density of states, probably dangling bond, near the dark Fermi-level. The questions that arise are: Can one relate the decrease in carrier lifetime directly to the measured increase in the density of deep states? Are the same metastable defects created uniformly in the i-layer of p-i-n structures as they are in films? To answer these, we studied electroluminescence (EL), transient current, and photocurrent before and after light-soaking in p-i-n structures.

Luminescence studies have proved to be one of the most successful means of exploring the detailed electronic properties of localized states. Photoluminescence (PL) explores the thin layer that is limited by the absorption depth. Electroluminescence (EL), on the other hand, is especially useful for studying localized states in p-i-n device structures. To study whether the bulk- or the interface-states are more important in recombination- and trapping-processes, we focused on EL and transient forward bias current as a function of device parameters such as thickness of the i-layer and p-i junction properties before and after photodegradation.

Based on the following experimental results, we suggest that EL can be used as a diagnostic tool for p-i-n solar cells.

(1) The EL spectral line shape is very sensitive to the cell structures, such as buffer-layer, thickness of i-layer, H-content and so on. For instance, we have found that in buffered p-b-i-n structures, the main-band luminescence was more pronounced than in simple p-i-n structures. This is an evidence that the recombination takes place near the p-i interface, because such a thin ($\approx 100 \text{ \AA}$) buffer layer would not contribute to luminescence signal directly but would improve the p-i interface. Further, the enhancement of the main-band luminescence relates with an increase of the open-circuit voltage, V_{oc} . This new understanding may help in the design of buffer layers.

(2) By varying the i-layer thickness, we studied where the recombination takes place. We found that the interface states contribute to low-energy recombination (gives "defect-band" luminescence) while the high-energy recombination (gives "main-band" luminescence) dominates in the bulk.

(3) By increasing the applied voltage, we moved the quasi-Fermi level position, that changes the recombination pathway. We have studied the correlation between the recombination pathway and the metastable-defects creation processes.

(4) EL spectral line shape is sensitive to light-soaking effects. We found that the high-energy recombination is more efficient in creation of metastable defects than is the low-energy recombination. Consequently, the thinner the i-layer, the less the SWE.

(5) Carrier recombination lifetime is an important parameter for solar cell performance. There is no single lifetime, but a wide distribution of lifetimes in amorphous semiconductors. Furthermore, from any other transport study, for instance, photoconductivity, or time-of-flight (TOF), one can obtain neither the lifetime nor the mobility separately; they appear always as the mobility-lifetime products (see Fig.15).⁵ However, from time-resolved EL study, we have measured the carrier lifetime distribution in real solar cell structures. We found that the carrier recombination lifetime consists of a fast component (peak at $\tau_f = 10^{-6}$ s), and of a slow component (peak at $\tau_s = 10^{-3}$ s) in 2- μm -thick p-i-n structures, and a single lifetime peaked at $\tau_f = 10^{-6}$ s in 0.4 - 0.5 μm p-i-n structures. Study of the light-soaking effects on lifetime distribution is under way.

RESULTS

A. Electroluminescence in a-Si:H p-i-n cells

1. Buffer-Layer Dependence of EL Spectra¹⁻³

It was found that a thin graded layer (buffer layer) at the interface between the wide band-gap p-layer and the intrinsic i-layer improves the cell properties by increasing the open-circuit voltage and the overall device performance. To explore the relation between the cell parameters and the fundamental physical processes, we have measured the electroluminescence (EL) spectra in these cells. The advantages of EL measurements compared with photoluminescence (PL) are (1) only non-geminate recombination takes place, because electrons and holes are injected from the n-i or p-i sides, respectively; and (2) recombination processes in both the bulk and the interfaces can be studied.

Table I Sample Preparation Conditions and Cell Performance

Solarex

Cell I.D.	Thickness (Å)	a-SiC p/i Buffer	Mode of Deposition	V _{oc} (volt)	J _{sc} (mA/cm ²)	Fill Factor	Efficiency %
S20330GD	2,100	none	rf PECVD	0.86	13	0.69	7.9
A2125-1	4,000	none	dc PECVD	0.81	~14	0.66	7.5
A2126-1	4,000	yes	dc PECVD	0.85	14.8	0.66	8.3

IEC p-i-n deposited by photo CVD

Cell	Thickness Å	C _H (at.%)	Buffer	Contact	V _{oc} (volt)	J _{sc} (mA/cm ²)	Fill Factor	Efficiency %
3282-11	5,300	11	none	ITO	.805-.815	12	0.65-0.67	6.5
3288-11	5,000	7	none	ITO/Ag	.798-.800	11.4-12.4	0.59-0.61	5.5-6
3355-21	5,500	7	yes	ITO/Ag	.840-.845	13.5-14.5	0.67-0.69	8-8.3

Thick p-i-n samples

Manufacturing	i-layer thickness(μm)	Top contact	Cell I.D.
APS	2.0	ITO	APS-1
SERI	2.0	Au	SERI-2
SERI	10.0	Cr	SERI-10

The p-i-n and p-b-i-n solar cells deposited on transparent conducting oxide (TCO) coated glass substrates were provided by Solarex and the Institute for Energy Conversion (IEC). The a-SiC:H buffer layer was about 150 Å thick. Ohmic contacts were made at the bottom and top electrodes by using Ag paint. The equipment for the EL measurements was described previously.^{1,2} The EL signal was collected from the glass side. A Ge detector for the EL spectra was used.

Figs. 1a and 1b show a comparison of the energy position shift between 0.4 μm - p-i-n and p-b-i-n cells made by Solarex at 300 K and 200 K. The curves with open circles and crosses correspond to p-i-n and p-b-i-n, respectively. The EL spectra contain two discernible bands: one at 0.85 eV ("defect band") and the other near 1.2 eV ("main band"). We observed more pronounced main band luminescence in p-b-i-n than in simple p-i-n structures, as shown in Figs. 1a and 1b. The EL main-band enhancement in p-b-i-n cells also has been found in 0.5- μm cells made at IEC, as shown in Fig. 2.

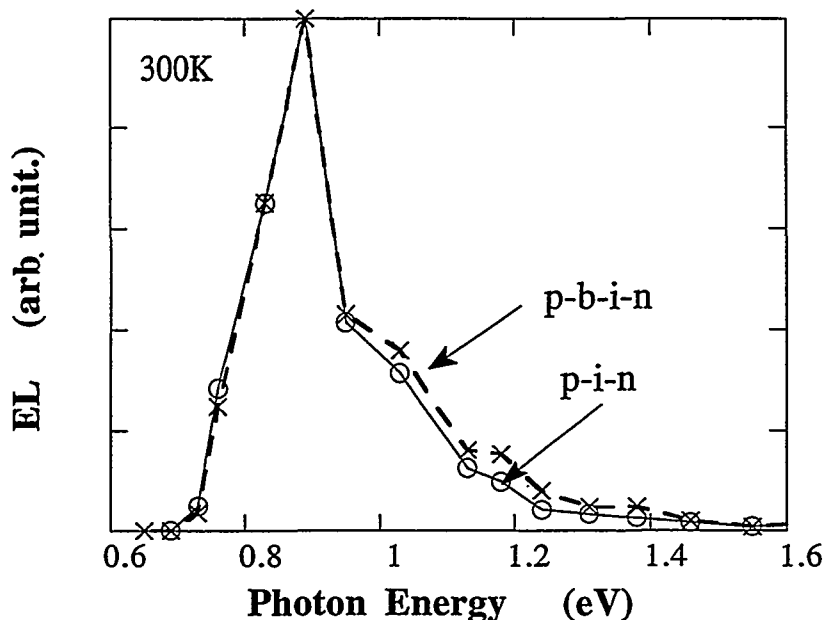


Fig. 1a Comparison of the EL spectra between buffered and non-buffered 0.4- μm solar cells at 300 K
 —○— A2125, p-i-n; —×— A2126, p-b-i-n.

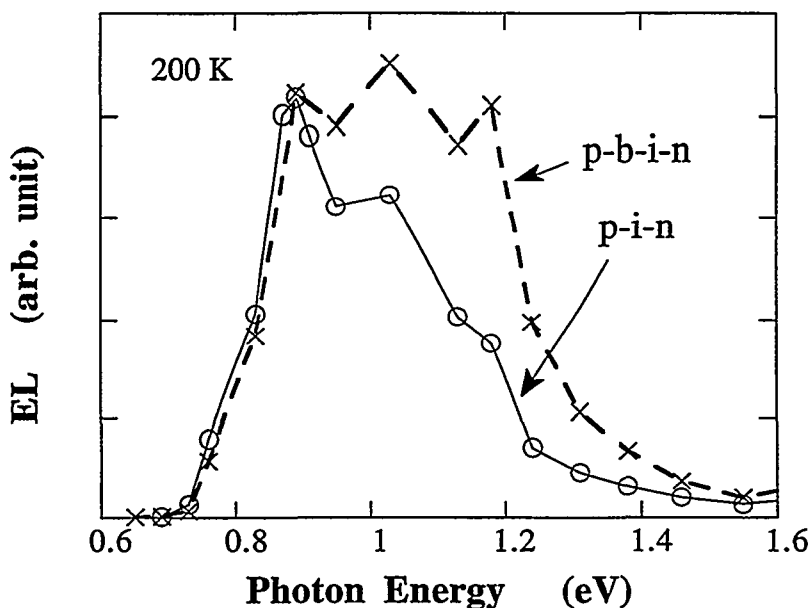


Fig. 1b EL spectra for the same group of samples as in Fig. 1a but at 200 K
 —○— A2125, p-i-n; —×— A2126, p-b-i-n.

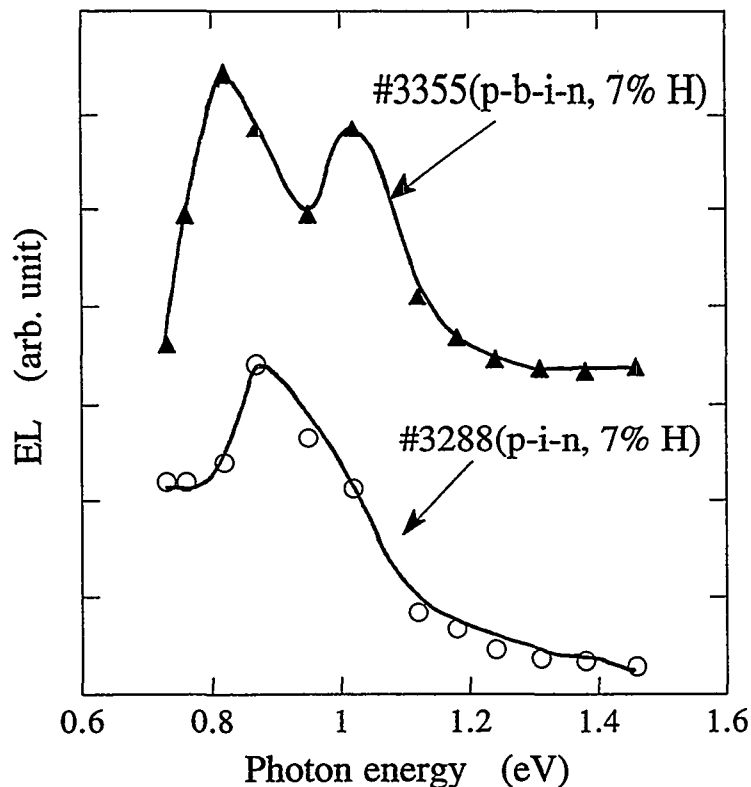


Fig. 2 EL spectra in 0.5- μm p-b-i-n and p-i-n cells at 300 K, applied voltage 0.9 V. Samples were made at IEC.

At 300 K, there are two discernible bands of the EL spectra: one at 0.85 eV ("defect band") and the other near 1.1 eV ("main band") in the p-b-i-n cells as shown by the upper curve in Fig. 2, but only one band peaked at 0.85 eV in the p-i-n cell, as shown by the lower curve in Fig. 2. One can see in Table I that the open-circuit voltage in p-b-i-n cells was 45 meV or 50 meV higher than that in p-i-n cells. It is clear that the more pronounced main-band luminescence is related to the increase in the open-circuit voltage. The comparison of light-soaking effects on buffered and non-buffered cells shows in A 5.

2. i-layer Thickness Dependence of EL Spectra^{3,4}

The sample parameters are listed in Table I. The EL spectrum is dominated by the 1.2-eV main band emission for the samples with thickness of 0.2 μm -10 μm at $T < 150$ K. With increasing temperature, there is a shift toward low-energy luminescence (~ 0.85 eV) in all samples as found in PL. However, thicker samples (≥ 2.0 μm) show significantly more main band emission (~ 1.2 eV) than thin samples.³ The EL spectra of the 0.2 μm sample show the lowest peak energy at 300 K. These results suggest to us that the "defect" luminescence dominates near the junction (probably at the p-i region) while the "main" band luminescence dominates in the bulk.

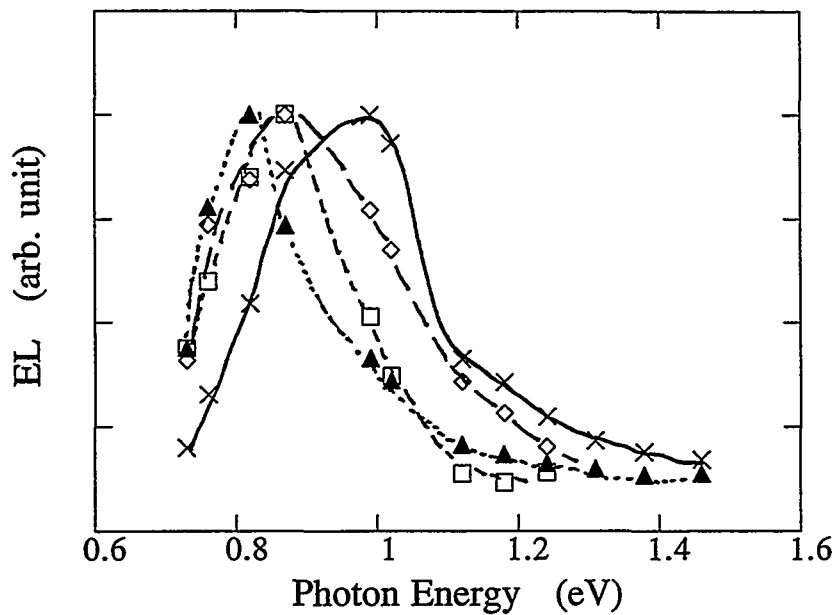


Fig. 3a Thickness dependence of EL spectra at 300 K

▲ S20330GD(0.2 μm) □ A2125-1(0.4 μm)
 ◇ NREL(2.0 μm) × NREL(10 μm)

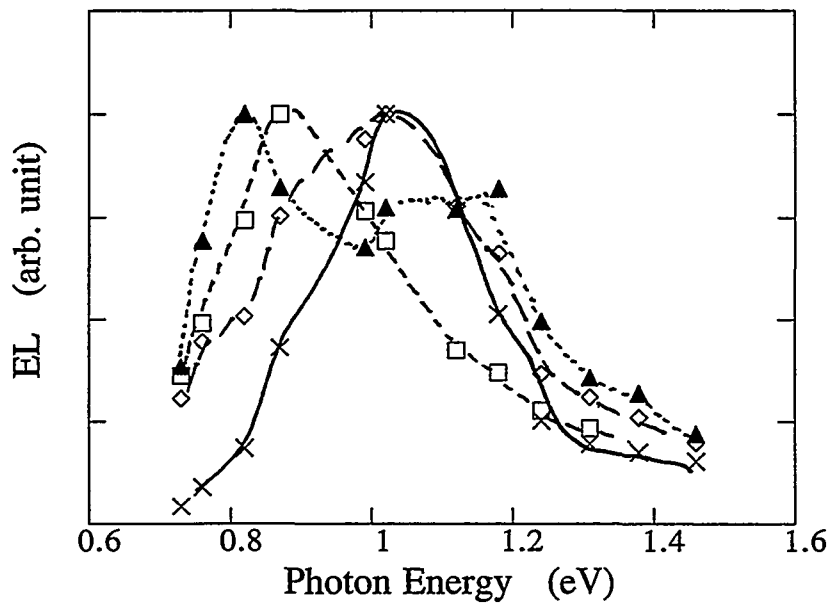


Fig. 3b Thickness dependence of EL spectra for the same group of samples as in Fig. 3a at 200 K

▲ S20330GD(0.2 μm) □ A2125-1(0.4 μm)
 ◇ NREL(2.0 μm) × NREL(10 μm)

One expects the density of defects to be higher near the junction region than in the bulk. The fraction of the volume occupied by the junction region is large in thin samples; consequently, the "defect" emission dominates. Figure 3a shows the thickness dependence of EL spectra at 300 K. The thin samples show more "defect" while the thicker samples show more "main" band

luminescence. Figure 3b shows the thickness dependence of EL spectra at 200 K for the same group of samples as in Figure 3a. Notice first that the EL peak energy shift is more obvious toward higher energy as the thickness increases from 0.2 μm to 10 μm ; second, the EL spectrum of the 0.2 μm sample shows a high energy 1.2 eV emission peak. The latter may originate from the carriers tunneling through the junctions and then recombining due to the higher electrical field.

3. Applied Voltage Dependence of EL Spectra

The applied voltage dependence of EL spectra has been observed in thin and thick p-i-n samples.^{3,4} Under higher electrical field ($\geq 1.5 \times 10^4$ V/cm), the EL spectrum contains a larger fraction of "main-band" emission; under lower electrical field ($\leq 5 \times 10^3$ V/cm), the EL spectrum shows a larger fraction of the "defect-band" emission. One group of results is shown in Figure 4a for 0.2 μm samples, and in Fig. 4b for 2.0- μm samples at 300 K. For the 0.2- μm samples in Fig. 4a, when the electric field across the i-layer increased from 5×10^3 to 9×10^4 V/cm, the EL main band around 1.2 eV showed an increase. For the 2.0- μm samples in Fig. 4b, when the electric field across the i-layer increased from 1×10^4 to 3.6×10^4 V/cm, the EL main band around 1.2-1.3 eV showed a more pronounced increase. One can understand this EL spectral line shape shift with increased voltage from the following simple argument: At a high current level, the quasi-Fermi level is high and located within the band tails. According to $\Delta E_f = kT \ln(j_2/j_1)$,

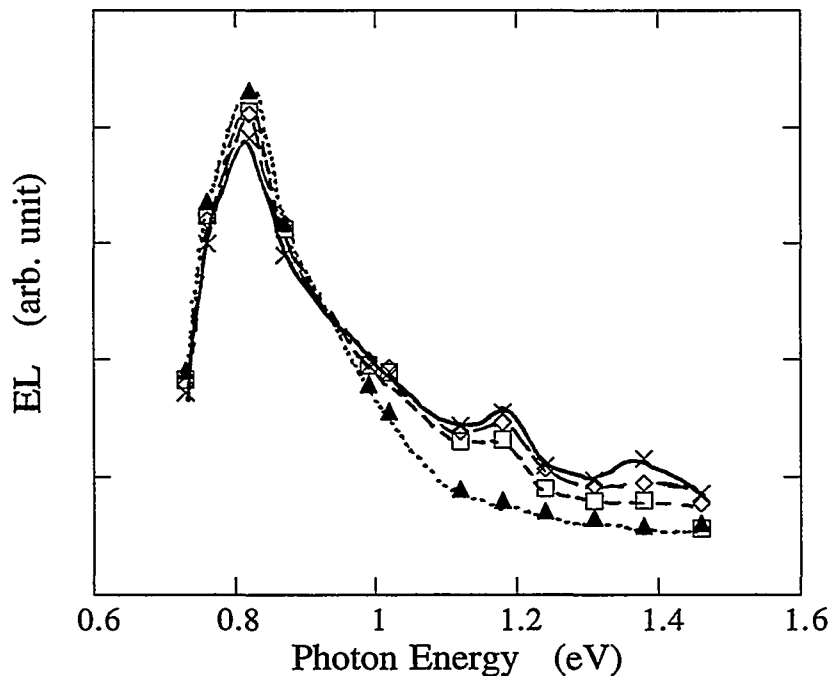


Fig. 4a Applied voltage dependence of EL spectra in a 0.2- μm p-i-n at 300 K
 \blacktriangle 0.8 V, \square 1.5 V, \diamond 2.0 V, \times 2.5 V.

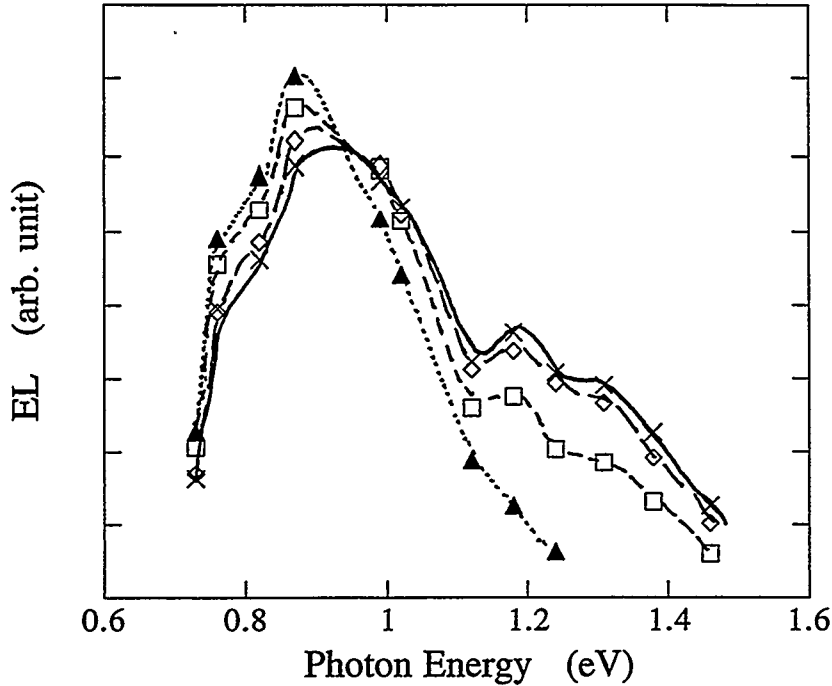


Fig. 4b Applied voltage dependence of EL spectra in a 2- μm p-i-n at 300 K
 \blacktriangle 2.7 V, \square 4 V, \diamond 6 V, \times 8 V.

the quasi-Fermi level position moved up about 45 meV and 60 meV in the 0.2- μm and the 2.0- μm samples, respectively. The higher the generation rate, the more probable is the high-energy band emission compared with the low-energy luminescence. This was not that clear in PL measurements, perhaps due to the surface emission domination in PL. Alternatively, these results may suggest that the "defect relaxation" takes place when the non-equilibrium carrier concentration increased.^{5,6} This means that the energy level of the defects moves up, so the emission photon energy increases.

4. EL Decay and Recombination Lifetime Distribution^{3,7}

Based on transient PL data, there is general agreement that for high quality a-Si:H, at the low temperature, low generation rate, lifetime distribution is dominated by a structure peaked at $\tau_s = 10^{-3} - 10^{-4}$ s, that τ_s shifts to shorter times with increased generation rate and temperature, and that τ_s is very sensitive to material quality.

We derive the lifetime distribution of a-Si:H from time-resolved transient EL measurements. The forward bias is applied with a programmable pulse generator (4×10^{-9} s fall time). A pulse width of 10 ms is used. A steady-state EL signal was observed after the double-injected current reached its steady-state value. The current falls rapidly when the pulse falls, while the EL signal shows a long decay due to the non-equilibrium electron-hole radiative recombination process. We find that the current decays instantly ($< 10^{-8}$ s) at all temperatures, but that the EL signal is first delayed until about 10^{-6} s and then decays more slowly. We detected the EL decay signal with a photomultiplier (1.1-eV cutoff energy, response time $\approx 10^{-8}$ s). An independent

measurement with a Ge detector (0.7-eV cutoff energy) was performed to confirm that the photomultiplier collects photons from the main luminescence band. We used 10 V at all temperatures except for $T < 150$ K where 14 and 20 V is also used to enhance the EL signal.

The decays of the EL signals are transformed into a lifetime distribution ϕ defined by

$$EL(t) = \int_{-\infty}^{\infty} d(\log \tau) \phi(\log \tau) \frac{\exp(-t/\tau)}{\tau} \quad (1)$$

We use

$$\phi(\log \tau = \log t) \cong t * EL(t) \quad (2)$$

which is a good approximation when the features of the distribution are broad.

The recombination lifetime distribution at several selected temperatures for a 2.0- μm p-i-n is plotted logarithmically in Figure 5. The distribution consists of a fast component whose peak occurs at $\tau_f = 10^{-6}$ s independent of temperature, and of a slow component whose peak position τ_s changes with temperature.

The existence of the slow and the fast peaks of the lifetime is further documented in Figure 6.

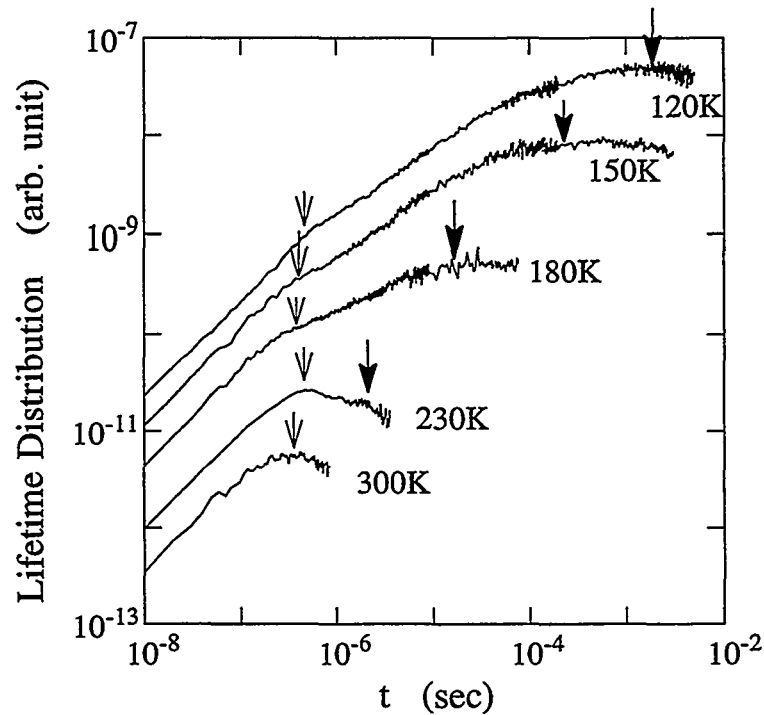


Fig. 5 Temperature dependence of lifetime distribution for a 2- μm p-i-n diode

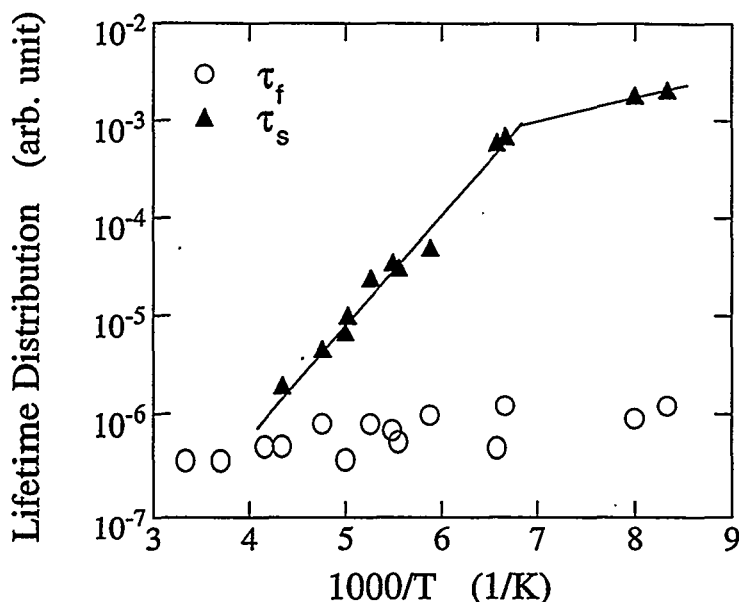


Fig. 6 The peak position of slow and fast lifetimes vs. $1/T$.
Data from the same sample as in Fig. 5.

In Figure 6, one can see that the slow lifetime τ_s becomes shorter as T is raised. This results from a transport-controlled rather than the nearest neighbor recombination. We suggested that the fast 10^{-6} s peak τ_f is due to nearest neighbor recombination because it does not vary with temperature.

As we have seen above, in 2.0- μm -thick samples there are two peaks of lifetime distribution (one at 10^{-6} s and one at 10^{-3} - 10^{-6} s), while in thin samples ($<0.5 \mu\text{m}$) we have only observed the fast peak. (See Fig. 9.)

5. Light-Soaking Effect on EL Spectra⁸

We report on the EL spectra as a function of photodegradation.² The light-soaked state B was reached by exposing the device through the glass side to a 2000 W/m^2 white light for 2 hours at room temperature.

Figures. 7a and 7b show the effect of photodegradation in a group of thin ($0.5\text{-}\mu\text{m}$) samples supplied by S. Hegedus of IEC at 300 K under 0.9 V and 3.0 V, respectively. Samples #3355, and #3288 were p-b-i-n (b-indicates a-SiC:H buffer-layer) and p-i-n in which the i-layers contain 7 at.% H. #3282 was a p-i-n device with 11 at.% H in the i-layer. One can see in Fig. 7a that the low-energy luminescence band dominates in the thin p-i-n samples #3288 and #3282, but some high-energy band is apparent in p-b-i-n sample #3355. There is not much of an effect of photodegradation in the p-i-n sample with 7 at.% H, but there is a decrease of "main band" EL with an increase of "defect band" EL in both the p-b-i-n sample and the 11 at.% H sample as shown in Fig. 7a. However, under higher voltage as shown in Fig. 7b, when the quasi-Fermi level moved into the tail states, there is a noticeable increase of the main-band luminescence. Again, there is more of a decrease of the main-band in both the p-b-i-n sample #3355 and the high-H sample #3282. This is consistent in that both the buffered sample and the high-H sample were less stable than the non-buffered and low-H samples.

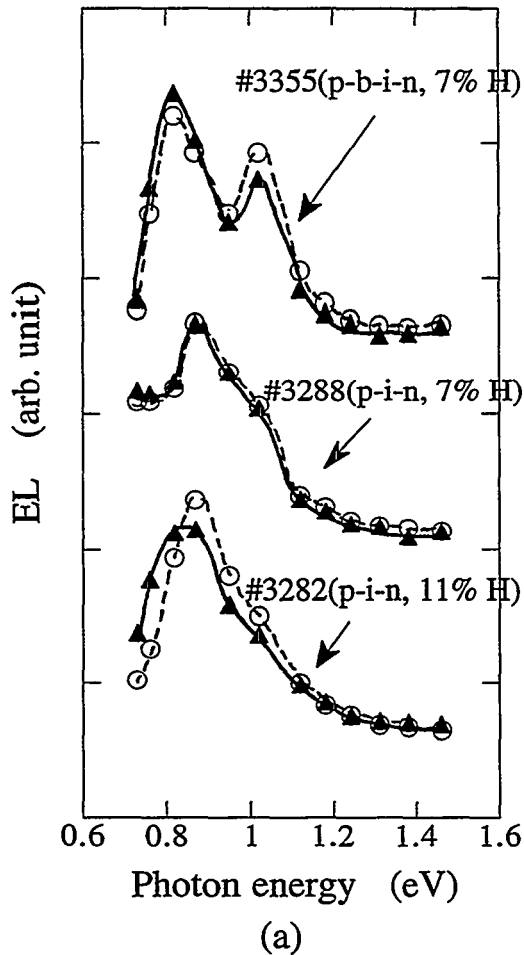


Fig. 7a Photodegradation on EL spectra in $0.5\text{-}\mu\text{m}$ samples at 0.8 V , 300 K . The open circles indicate original state A, the triangles light-soaked state B.

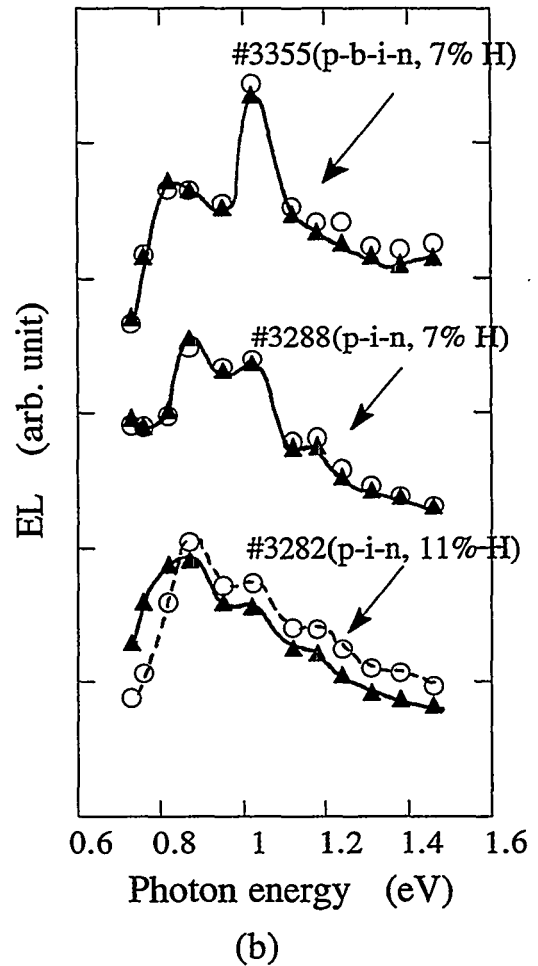


Fig. 7b Photodegradation on EL spectra in $0.5\text{-}\mu\text{m}$ samples at 3 V 300 K . The open circles indicate state A, the triangles state B.

In order to examine whether the degradation takes place near the junction or in the bulk, we have studied degradation in thick samples ($2.0\text{ }\mu\text{m}$). These results at 300 K are shown in Fig. 8. Clearly, the photodegradation effect in thick samples is more pronounced than that in thin samples. Again, what is observed is that the intensity of the high-energy band is reduced and the low-energy band is increased.

It is worth mentioning here that when the "main band" is more pronounced, either in the p-b-i-n sample or at higher applied V , the photodegradation of this band is more obvious. So it is reasonable to surmise that the Staebler-Wronski effect is due to the high-energy (1.2 eV) recombination, and it is not directly related to defect-controlled recombination. In thin samples ($\leq 0.5\text{ }\mu\text{m}$), defects dominate the recombination, so the Staebler-Wronski effect is either smaller or slower because only a very small fraction of the recombination involves the band tails.

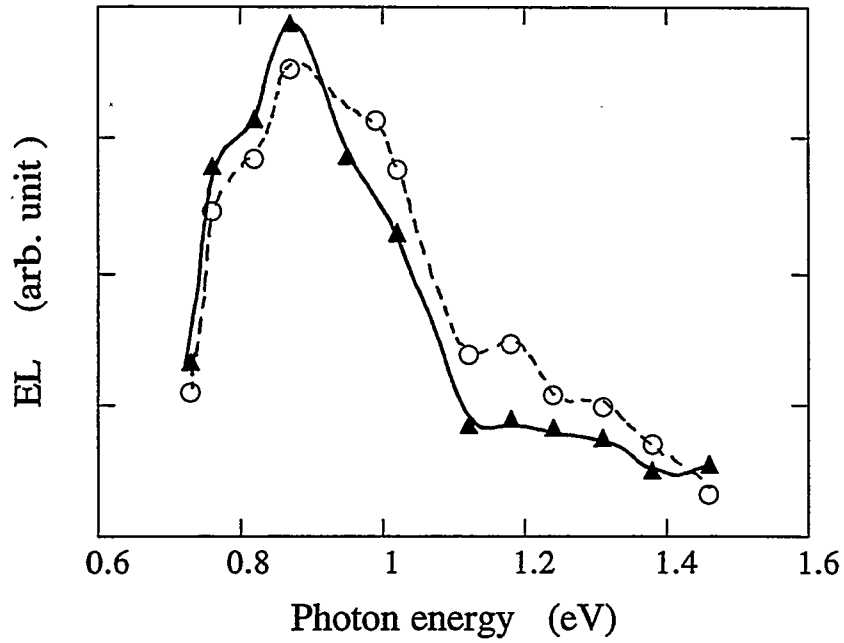


Fig. 8 Light-soaking effect on EL spectrum in a 2- μm p-i-n under 4V at 300 K

6. Light-Soaking Effect on EL Decay ^{3,8}

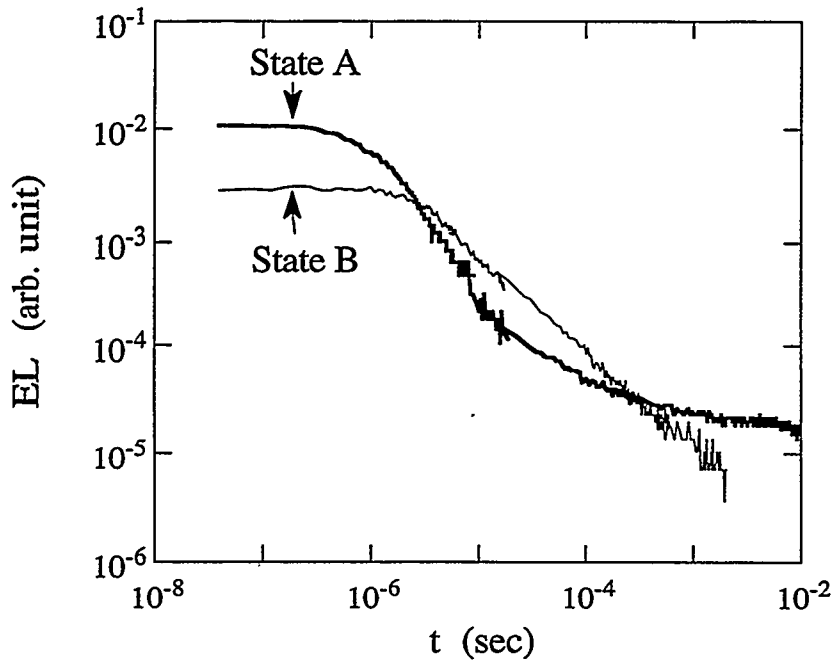


Fig. 9a Photodegradation effect on transient total EL decay, in a 0.4- μm p-i-n after a 4 V pulse at 100 K

We have examined the light-soaking effect on recombination lifetime distribution. In Fig. 9a we show the EL decay vs. time in the annealed state A and light-soaked state B in a thin (0.4- μm) p-i-n at 100 K. The EL signal delay is longer and decay is much slower in state B than in state A. This implies a broad distribution of lifetimes in light-soaked state B. The lifetime distribution $\tau \approx \text{EL} * t$ is shown in Fig. 9b. One can see a peak, $\tau \approx 1 \mu\text{s}$ in state A, but a broad distribution for $\tau > 3 \mu\text{s}$ in state B.

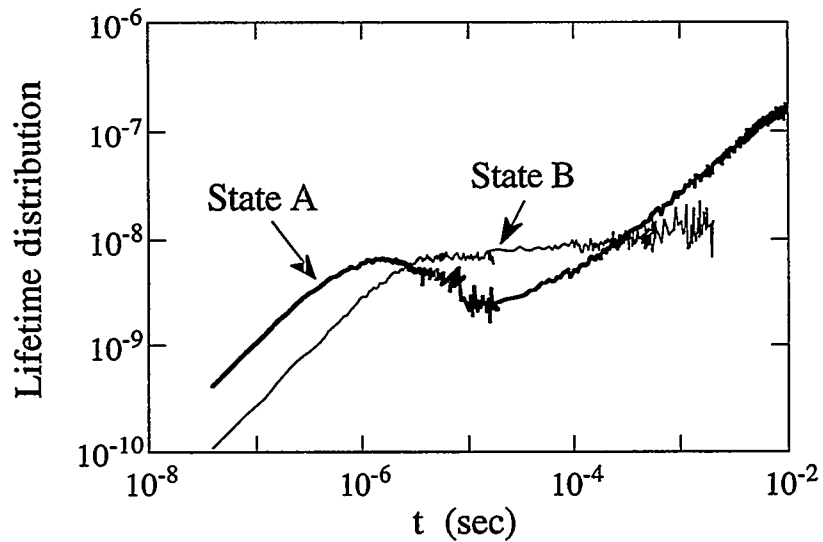


Fig. 9b Photodegradation effect on lifetime distribution deduced from Fig. 9a, as $\tau \sim \text{EL} * t$

7. Conclusions

The main conclusions that we draw from these EL studies are

- 1) Defect luminescence is mainly a junction effect. One often observes the defect PL band at higher temperature; PL is probably mainly a surface effect at those temperatures. However, we have both the interface and the bulk luminescence signals in EL studies, so we have observed more pronounced "main-band" luminescence. Furthermore, the higher the applied voltage, the more the "main-band" EL appears, even in thin samples.
- 2) "Main-band" luminescence is a true i-layer bulk effect, which is why it is easier to observe in thick samples than in thin ones.
- 3) EL can be used as a diagnostic tool not only to study bulk and junction-controlled recombination, but also to realize where and how the light-induced defects are created in p-i-n cells.
 - * The EL spectral line shape is very sensitive to the cell structures. We found that in buffered p-b-i-n structures, the main-band luminescence was more pronounced than in simple p-i-n structures. This is an evidence that the recombination takes place near the p-i interface, because such a thin ($\cong 100 \text{ \AA}$) buffer layer would not contribute to luminescence signal directly but would improve the p-i interface. Further, the enhancement of the main-band luminescence related with an increase of the open-circuit voltage, V_{oc} . This new understanding may help in the design of buffer layers.
 - * By varying the i-layer thickness, we found that the interface states contribute to low-energy recombination while the high-energy recombination dominate in the bulk.
 - * By increasing of the applied voltage, we have studied the correlation between the recombination pathway and the metastable-defects creation processes.
 - * EL spectral line shape is sensitive to light-soaking effects. We found that the high-energy recombination results more efficient in a creation of metastable defects than the low-energy recombination. Consequently, the thinner the i-layer, the less the SWE.
 - * Carrier recombination lifetime distribution in real solar cell structures has been studied by transient EL. We found that lifetime consists of a fast component (peak at $\tau_f = 10^{-6} \text{ s}$), and of a slow component (peak at $\tau_s 10^{-3} \text{ s}$) in 2- μm -thick p-i-n structures, and a single lifetime peaked at $\tau_f = 10^{-6} \text{ s}$ in 0.4 - 0.5 μm -thick p-i-n structures.

B. Light-soaking Effects on Transient Current in a-Si:H p-i-n cells⁹⁻¹¹

Transient forward bias currents in a-Si:H p-i-n devices give information on the quality of the contacts, the quality of the junctions, the density of states, and the electron trapping and recombination in the i-layer. Transient forward currents have shown general features of a decaying initial space-charge-limited current (SCLC) followed by a delayed rise of the current to values generally higher than the initial SCLC. The rise is attributed to the transition from SCLC to recombination-limited current (RLC). It has been found that the $I(t)$ curves depend on the pulse repetition rate, the applied voltage, the sample temperature, and its illumination history.¹⁰ The SCLC region in p-i-n devices is consistent with that observed in n-i-n devices.⁹ However, no fast-trapping processes of the current transient in both n-i-n and p-i-n structures have been found.^{9,10} Moreover, a relaxation time as long as 10^4 s was found after injecting carriers in p-i-n samples.¹² This slow decay of SCLC and long time recovery can not be solely attributed to either deep trapping or emptying from rigid defect states. Instead, a defect-relaxation model has been suggested.^{2,5}

To gain more insight into the mechanism, we have examined in detail the i-layer thickness, pulse repetition rate, and reverse bias effects in a-Si:H diodes. These results along with photodegradation effects are presented and discussed below.

1. Repetition Rate Dependence of Transient Forward Bias Current in p-i-n cells¹⁰

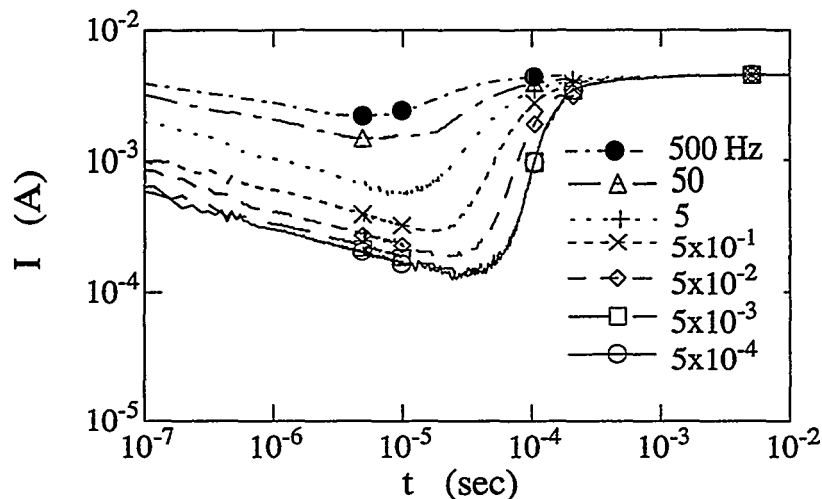


Fig. 10a Pulse repetition rate dependence of $I(t)$ in a $10\text{-}\mu\text{m}$ p-i-n at original state A

Figures 10a and 10b show the pulse repetition rate dependence of the $I(t)$ in a $10\text{-}\mu\text{m}$ thick p-i-n in state A and in state B, respectively. The data were taken with 1×10^{-2} s width, 12 V pulses at 20°C . At the lowest repetition rate of 5×10^{-4} Hz, the sample was close to its steady-state configuration between pulses. At high repetition rate, the initial SCLC can be ten times larger, and the delay of RLC rise is shorter than that for low repetition rate. The SCLC decays as a power law $I(t) \propto \mu\tau^{-(1-\alpha)}$. Comparing the $I(t)$ curves between states A and B, one sees that the SCLC decay is faster and the delay of the RLC rise is longer in state B than in state A. A small over-shoot of the RLC occurs in state B; this is related to an increase of deep traps.

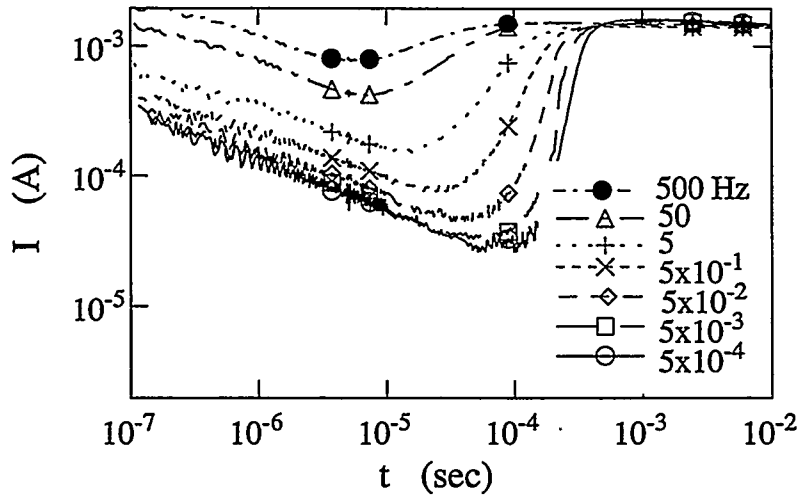


Fig. 10b Pulse repetition rate dependence of $I(t)$ for the same sample at light-soaked state B

A much smaller repetition rate effect is found in $0.4\text{-}\mu\text{m}$ samples. There is no obvious change of the $I(t)$ curves after exposing the sample to 2000 W/m^2 white light for 2 hr. These results are shown in Fig. 11. The data were taken at state A with 1.5-V pulses at 20°C . The $I(t)$ curves show a slight delay of the RLC rise (not shortened as in thick samples) from 1×10^{-6} to 1.2×10^{-6} s with an increasing repetition rate from 1×10^2 to 1×10^4 Hz. There was almost no change from 1×10^{-4} to 1×10^2 Hz, and above 1×10^4 Hz.

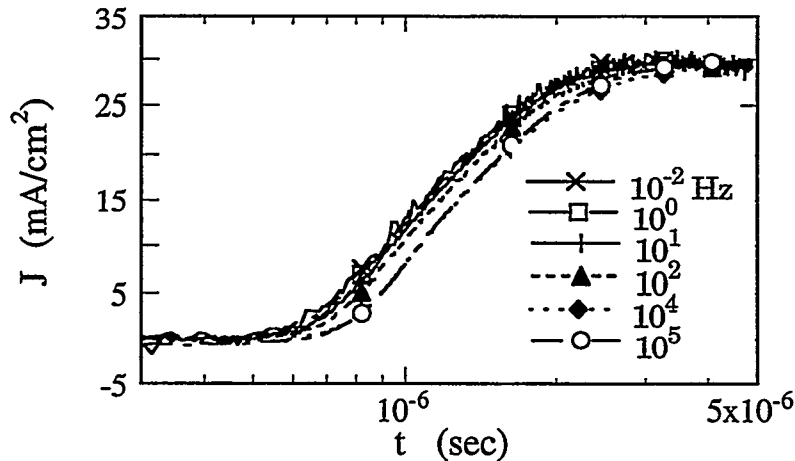


Fig. 11 Pulse repetition rate dependence of $I(t)$ in a $0.4\text{-}\mu\text{m}$ p-i-n at 300 K

The pulse repetition rate dependence in $0.4\text{-}\mu\text{m}$ samples shows a typical junction capacitance behavior. The junctions can be recovered between 10 Hz pulses. When the pulse frequency is higher than 10 Hz, the p-i (n-i) junction capacitance can not follow it, which makes the current delay slight as shown in Fig. 11. However, for thick samples, unlike in thin samples, the Fermi-level is pinned in the middle of the gap, but the quasi-Fermi level in the i-layer varies with the density of the non-steady-state carriers. The $I(t)$ curves in Fig. 10 can be explained by the higher repetition rate the more carriers in the i-layer left from the previous pulse, which accounts for the higher value of the SCLC and the smaller delay of the RLC rise. A repetition rate lower than 10^{-4} Hz is required for the thick samples to reach their steady-state configuration between pulses.

2. Reverse Bias effects on Transient Forward Current in p-i-n^{2,3,10}

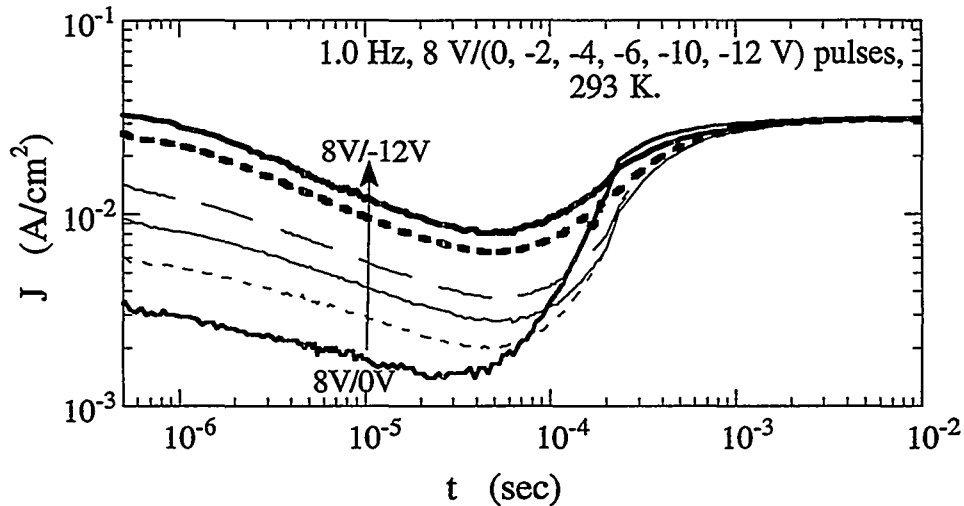


Fig. 12a Negative bias dependence of forward current on a 10- μm p-i-n diode at State A

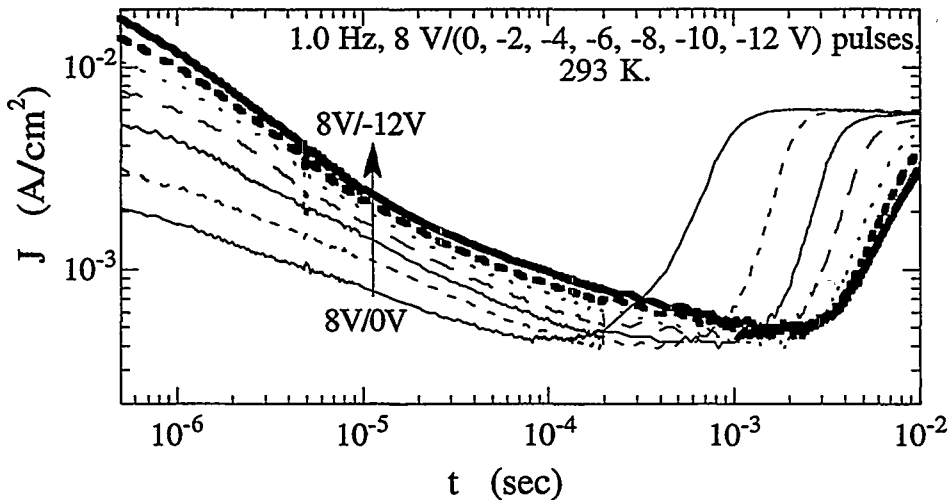


Fig. 12b Negative bias dependence of $I(t)$ for the same sample as in Fig. 12a at State B

We applied a negative bias between the positive pulses to gain more insight into the mechanism of the transient current in a-Si:H p-i-n. We found a profound effect on the transient response in samples $\geq 2 \mu\text{m}$. The typical curves are shown in Figs. 12a and 12b for a 10- μm sample in state A and state B. The data were taken with 1.0-Hz, 8-V positive pulses and a 0 to -12 V negative pulse in between. The reverse bias gives a higher initial SCLC and a longer delay time of RLC rise. A significant delay was found in state B. This is 1.5×10^{-4} s and 3×10^{-3} s at 0 and -12 V negative bias, respectively, as shown in Fig. 12b. One might expect a larger initial current due to positive charges left from the reverse bias; however, one would have expected this initial current to decay faster before the rise and the delay of the RLC rise to be shortened (as seen in Figs. 10a and 10b). This is contrary to what is observed.

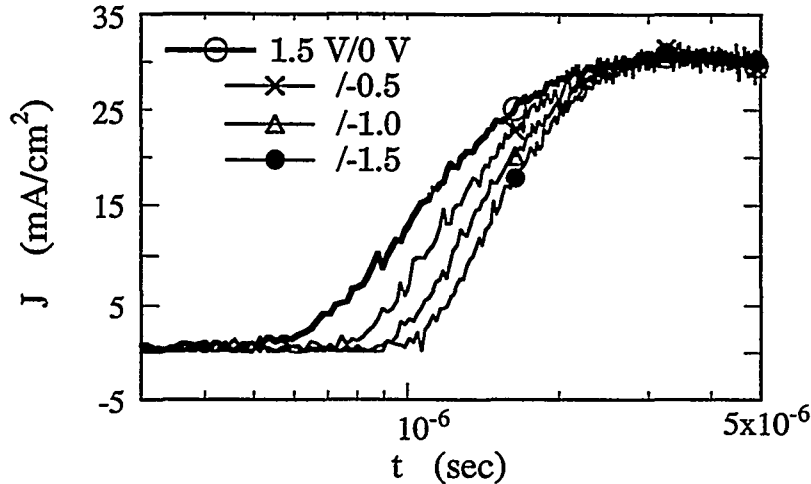


Fig. 13 Negative bias effect on transient current $I(t)$ in a $0.4\text{-}\mu\text{m}$ p-i-n at 300 K in state A

In $0.4\ \mu\text{m}$ samples little reverse bias effect is found, as shown in Fig. 13. The data were taken with 1.0 Hz, 1.5 V positive pulses and a 0 to -1.5 V negative pulse in between. Compared with thick samples, we infer therefore that the repetition rate and negative bias effects are mainly due to the bulk and not to the junction.

The most interesting result of the transient response is the reverse bias effect in thick samples ($2\text{-}10\text{-}\mu\text{m}$ p-i-n have been studied).^{2,10} The most pronounced effect was observed at state B (as shown in Fig. 12b) where the samples have more defects near the p-i junction than in the i-layer. These metastable defects make for a long delay time of the RLC at 3×10^{-3} s when a -12-V bias was applied between the 8 V pulses. In $0.4\text{-}\mu\text{m}$ thin samples, a similar but much smaller effect was obtained (Fig. 13). We suggest that, under reverse bias, the electrons are extracted from the i-layer, which creates more positive charged defects and/or holes in deep valence band tail states. This positive space charge will not empty rapidly so that, upon application of the forward bias, it adds to the internal field giving a much larger initial SCLC. This idea is attractive in that it would explain why little reverse bias effect is found in thin samples; that is, in this sample the space charge already completely fills the volume and little effect would be observed. Unfortunately, there is a serious difficulty with this proposal because, in a few electron transit times ($\approx 10^{-6}$ s), the electrons would neutralize the positive space charge and the reverse bias effect would disappear in about 10^{-6} s. So far, the results cannot be fitted by any computer simulations. A new mechanism besides the traditional SWE model must be involved in the light-soaking effect of a-Si:H p-i-n structures.

An addition, upon neutralization of the positive space charge by the electrons, the charged defects are in their non-equilibrium configuration. (Branz and Schiff et al.⁶ have proposed exactly such a model.) This leaves the captured electrons in a very high energy state raising the quasi-Fermi level. This quasi-Fermi level decays very slowly with atomic relaxation times, giving rise to a much larger SCLC until recombination takes place. (A similar effect was found in transient photoconductivity by Han et al.⁵) Consequently, the rise time of the RLC must be delayed some more while neutralization of the positive space charge clearly takes place. If these ideas are correct, then one cannot use simple Shockley-Read recombination to calculate forward bias- and photo-currents in a-Si:H, because the relaxation ideas must be included.

3. Slow Relaxation Processes¹⁰⁻¹²

Carrier transport properties, including the mobility-lifetime product, $\mu\tau$, are important parameters for the understanding of the electronic properties of a-Si:H devices. We have attempted to study these parameters by the decay of the forward current. In order to obtain a better grasp of the recombination mechanism for excess carriers due to forward bias in a-Si:H p-i-n diodes, we have studied the decay of the excess charge by a variety of related experiments.^{5,10,12} The results of forward current decay for a 2 μ m diode are shown in Figure 14. Two methods were used to obtain the current decay data.

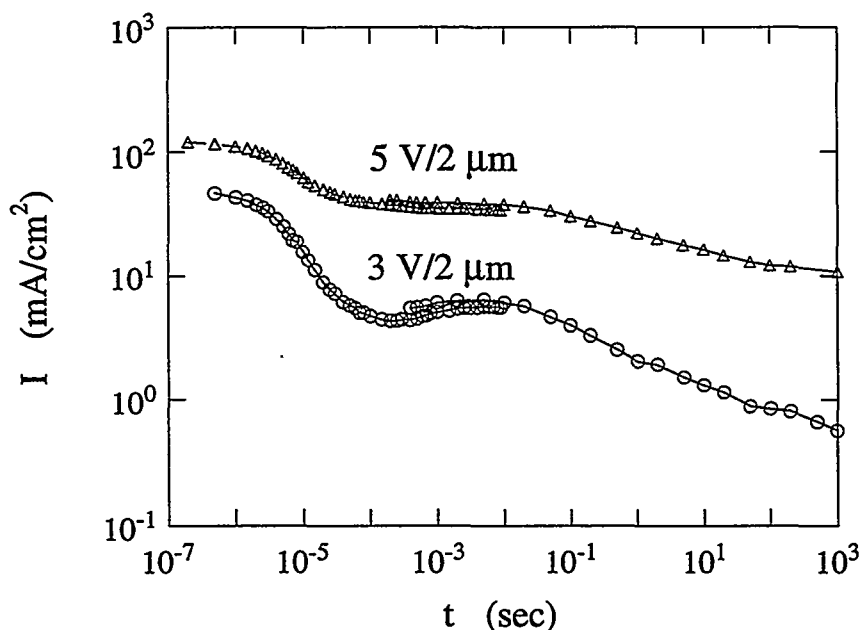


Fig. 14 Forward current decay in a 2- μ m p-i-n diode at 300 K. The data were taken by 3 V/0 V/3 V and 5 V/0 V/5 V pulses.

At $10^{-7} \text{ s} < t < 10^{-2} \text{ s}$ we measured the frequency dependence of the amplitude of the forward current; at $10^{-4} \text{ s} < t < 10^3 \text{ s}$ we used a dual-pulse method in which the pulses sequence as positive/zero/positive. Because the forward response consists of a decrease of space charge limited current and then rise of recombination current, there is a current minimum which indicates the forward current decay of the first positive pulse response. We can see that the data from two methods overlap at $10^{-4} \text{ s} < t < 10^{-2} \text{ s}$. The similarities between these two method of indicates that the relaxation time is very long, longer than 10^3 s . What is interesting about the forward current decay results is that there are clearly four sections of the decay curves. First there is a flat part, when $t < 10^{-6} \text{ s}$, then a relatively fast drop starting at about $1 \times 10^{-6} \text{ s}$ to $5 \times 10^{-5} \text{ s}$, and the drop is steeper at lower applied voltage. After that, there is a plateau from 5×10^{-5} to $1 \times 10^{-2} \text{ s}$, followed by a slow decay again. It is clear that the apparent decay of the excess charge is very slow, that in many cases more than 10^4 s is needed for the sample to completely recover from the forward bias injection. This is such a long time that it is difficult to attribute it to pure one-electron decay of deep rigid centers either by emptying or recombination. Furthermore, the so-called deep-trapping process has not been seen in our transient current measurements.^{9,10,12} Perhaps, a slow relaxation of the deep traps contribute to these mystery.^{2,5,6}

Slow relaxation may also be inferred from a comparison of the transient charge collection with and without optical bias.⁵ These results are shown in Figure 15.

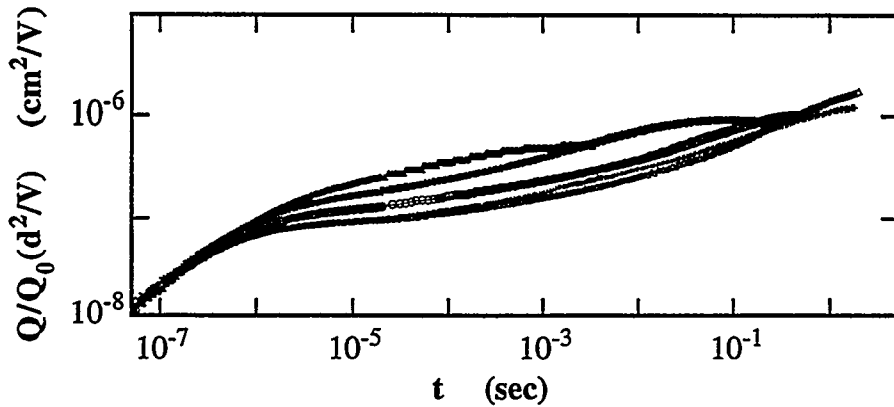


Fig. 15 The transient photocharge $Q(t)/(d^2/Q_0V)$ recorded at four optical bias levels and in the dark in an a-Si:H specimen in a light-soaked state. The dc currents through the specimen were 2.7×10^{-7} A, 1.8×10^{-8} A, 1.0×10^{-9} A, 4.8×10^{-10} A, and 5.0×10^{-11} A, from the top to the bottom curves.

The collected transient photocharge $Q(t)$ has been normalized by (d^2/Q_0V) , where d is the separation between two electrodes, Q_0 is the photogenerated charge, and V is the applied voltage across the electrodes. Because $Q(t)/(d^2/Q_0V)$ equals to $\mu\tau$, one can obtain several parameters, such as deep-trapping lifetime, re-emission time, and recombination lifetime, from these curves.⁵ The signature of deep trapping in a charge collection experiment is an "S" shape. Such a shape is observed only for bias light currents less than 10^{-8} A, which means that the quasi-Fermi level is at most 0.1 eV higher than the dark Fermi level, which yields a current of 5×10^{-11} A. Notice that the deep trapping process between 10^{-6} - 10^{-3} s is apparent from the "S" shape of the charge collection response as shown by the bottom curve in Fig. 15. On the other hand, the deep trapping is suppressed with optical bias. We believe that this results from a shift in energy between the relaxed and unrelaxed defect states, which is due to the optical bias excitation.

4. Conclusions

(1) The forward-bias-transient-current in p-i-n cells shows that unlike in a-Si:H films,¹⁰ there is no evidence for the so-called deep-trapping process in p-i-n structures as shown in Fig.10.

(2) In 0.4- μm -thick samples the junctions can be recovered within 10^{-1} s (or 10 Hz pulses); for thick samples ($\geq 2\mu\text{m}$) to reach their steady-state configuration requires longer than 10^3 s (or 10^{-4} Hz pulses). So we conclude that the junctions recover faster than the bulk when subjected to excess carriers due to bias.

(3) The recombination current rise time after light-soaking is more than one order of magnitude longer than before light-soaking, but the final current did not change much. Defect-relaxation is suggested to explain the slow response in light-soaked state B. Slow relaxation was also observed in optical bias measurements in a-si-hn films. So we conclude that the slow relaxation is a bulk effect.

C. Light-soaking Effect on Photo-gain in a-si-h n-i-p cells^{13,14}

1 Experimental results

Finally, we have some data, obtained in collaboration with R. Vanderhagen of The Thin Film and Surface Physics Lab at Palaiseau, France, on forward bias dark and photocurrent. The experimental results were obtained with an apparatus as described previously.¹³ Researchers prepared n-i-p samples at Palaiseau. A good injecting contact was checked by varying the interfaces and device annealing. For photocurrent studies, the light source was a 632.8-nm laser. Neutral density filters were used to vary the incident flux F . When the laser was used for light degradation (open circuit), the photocurrent was 33 mA/cm^2 , corresponding to an equivalent photodegradation under AM10 sunlight. The forward bias photocurrent was obtained after subtraction of the dark current from the total current with light excitation. The built-in potential was found from the forward bias current vs. applied voltage (J_d vs. V_a) data, and $V_{bi} = 0.7 \text{ V}$ has been subtracted from the applied voltage to obtain the voltage across the i-layer, $V = V_a - V_{bi}$. The following curves were from various $1 \mu\text{m}$ n-i-p samples. We concentrate on $1\text{-}\mu\text{m}$ thick devices because the photogeneration and the lightdegradation are nearly uniform. Figure 16 shows the forward bias dark- and photo-current vs. V on $1\mu\text{m}$ n-i-p cell before and after light-soaking.

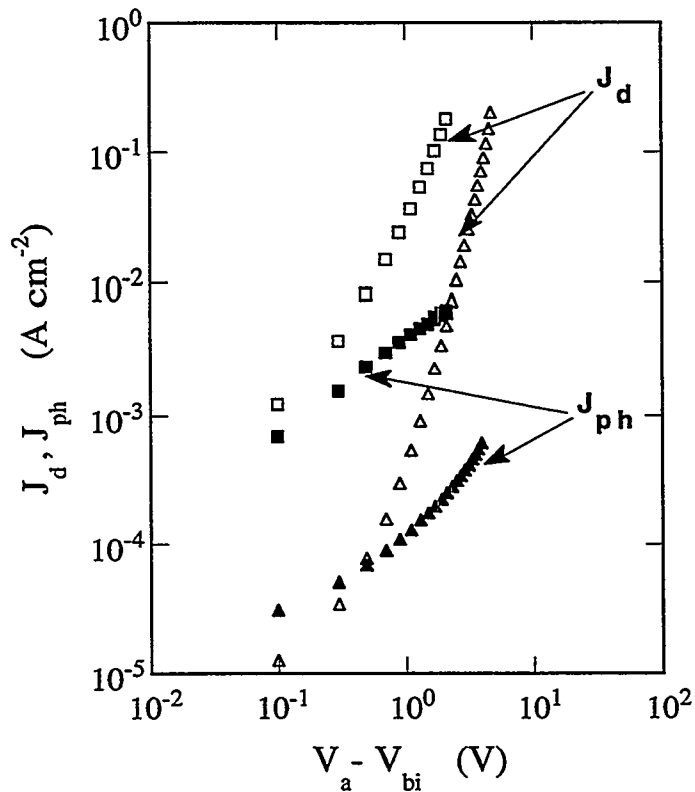


Fig 16 Forward bias dark current and photocurrent vs. $V_a - V_{bi}$ for a $1\text{-}\mu\text{m}$ n-i-p diode before and after light degradation. Squares and triangles indicate before and after degradation.

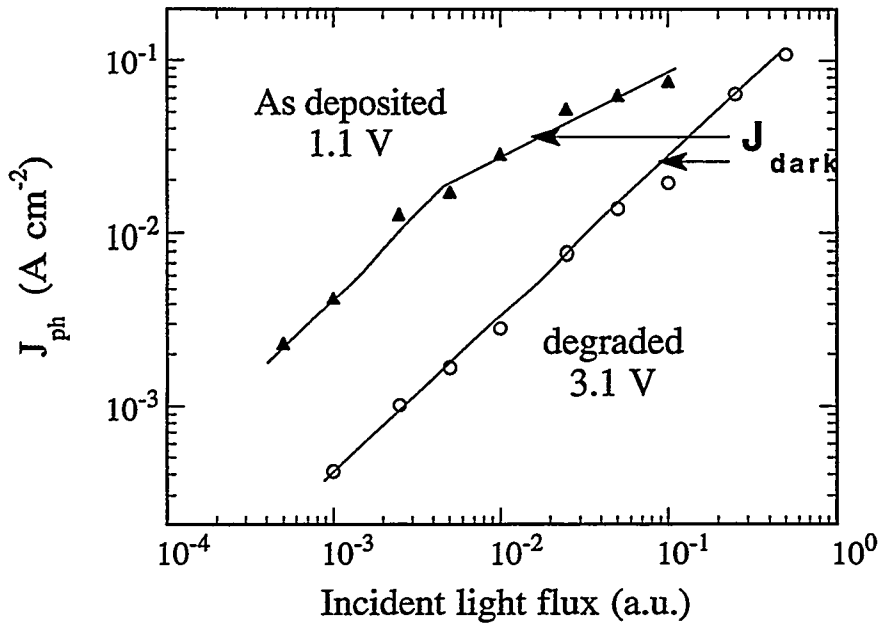


Fig. 17 Forward photocurrent vs. photo-flux in $1 \mu\text{m}$ n-i-p. Triangles and squares correspond to undegraded and light-degraded states. The dark current is indicated.

Figure 17 gives photocurrent as a function of incident flux before and after light-soaking for the same sample in Figure 16.

Photocurrent under forward bias compared with reverse bias photocurrent yields the photo-gain $j_{\text{ph}}^{\text{F}} / j_{\text{ph}}^{\text{R}} = G_{\text{ph}}$ directly. Recently, in annealed a-Si:H n-i-p devices, we showed that photo-gains of greater than 500 under forward bias can be achieved.^{12,13} This implies that the lifetime is longer than the transit time in those 1-3- μm thick p-i-n samples.

We have studied the effect of photodegradation on the forward bias photo-gain in a-Si:H n-i-p devices. Our data show that often bimolecular recombination dominates at high current density, and degradation of the photo-gain follows a power-law of $t^{-1/3}$.

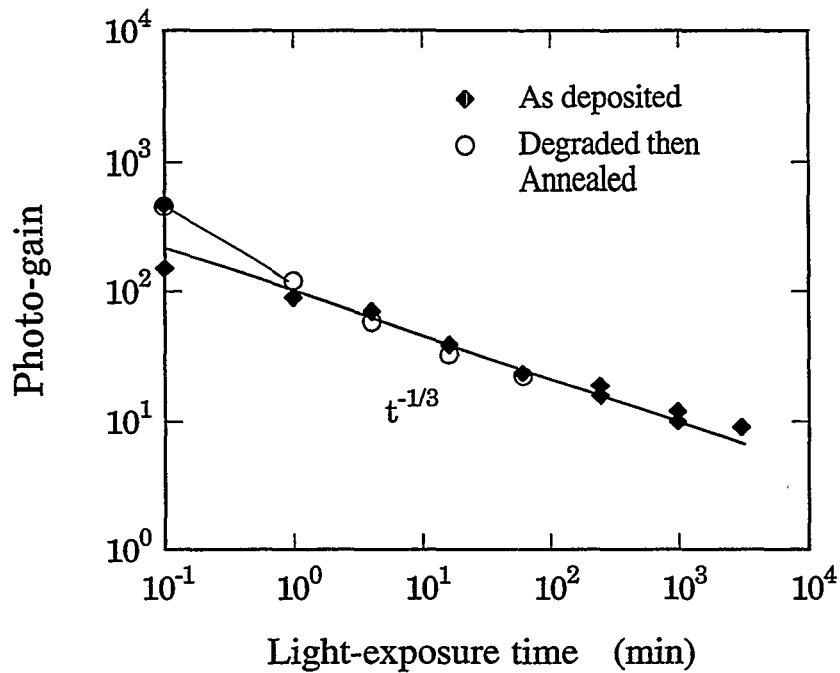


Fig. 18 Photo-gain as a function of AM10 light degradation time. Open circles indicate a sample partially annealed (140 °C, 1 hr) and degraded again.

Figure 18 shows the dependence of the photo-gain as a function of the degradation time for the as-deposited sample and for a reversible degraded-annealed sample (annealing at 140°C). The gain follows a power law of $t^{-1/3}$, the same as was observed for the bulk sample from constant photocurrent method (CPM). This is expected when the lifetime is controlled by the deep states but there is a small fraction of bi-molecular recombination. At early time $t < 1$ min, the degradation was much faster in the as-deposited sample, and the 140°C annealing did not fully recover the photo-gain to its "as-deposited" value.

2. Conclusions

The photo-gain measurements is a direct method to study the $\mu\tau$ product in real device structures. It can also be used to study the light-induced metastable defects. So far we have only succeeded to measure n-i-p structures, but not p-i-n structures, because the gain factor depends on the junction injection. We do not know how to handle the problem of junction limitation now.

D. Theoretical Results

1. A Simple Model of Recombination Current and EL in a-Si:H¹⁵⁻¹⁸

Over the past several years, we have developed a phenomenological model for double injection.¹⁸ Because EL represents some fraction of the recombination current, this simple model can be applied to it as well. To evaluate the recombination current, the current flow in the circuit can be written as

$$\nabla \cdot \mathbf{J} = g - \nabla \cdot \mathbf{J}_r \quad (3)$$

where \mathbf{J}_r is the recombination current and g is the effective generation rate. Integrating over the entire volume of the diode one has

$$I_{out} - I_{in} = \frac{CV}{t_0} - I_r \quad (4)$$

where C is the geometric capacitance of the diode and t_0 is the effective transit time of the carriers.⁷ Now from Eq. (4), because both I_{in} and I_{out} must be equal to the circuit current carried by free electrons and free holes, $I_{fn} + I_{fp}$, one has $I_r = CV/t_0$ in steady state. The meaning of this is that the recombination current adjusts itself through the population of recombination centers so that $CV/t_0 = I_r$ at steady state.

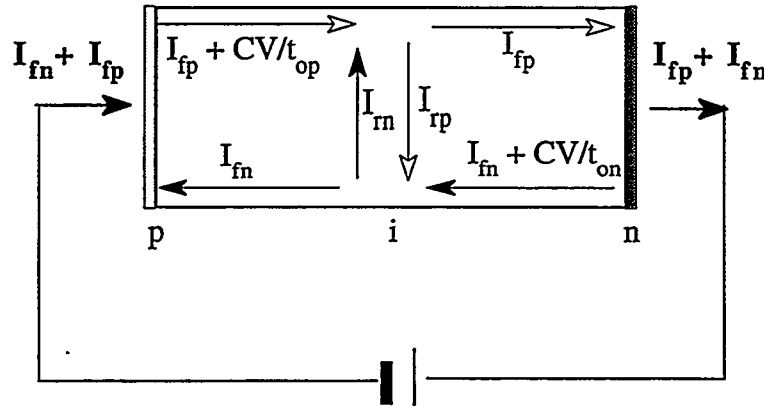


Fig. 19 Schematic plot of the electrons and holes flow through a p-i-n diode

Figure 19 is a schematic plot of the current flow through a p-i-n diode. Computer simulations are needed for solving a complete set of kinetic equations for the holes and electrons; however, to give a semi-quantitative picture, we use the equivalent diagram shown in Fig. 19. Both the hole and electron injection currents are contained in the term CV/t_0 . When there is gain in the circuit, $G \equiv \tau/t_0$, where τ is the lifetime of the carriers, one obtains the current approximately as

$$I_f = \frac{CV}{t_0} G = I_f \frac{\tau}{t_0}. \quad (5)$$

This means that the recombination current is τ/t_0 times smaller than the forward bias current. We have argued^{16,17} that one should not use $\eta^* = EL/I_f$ as the EL efficiency, but $\eta = EL/I_f = \eta^*(\tau/t_0)$. We should also be note that the radiative-lifetime τ_L is larger than the non-radiative-lifetime τ , the EL efficiency, therefore is $\eta = \eta^*(\tau_L/t_0)$, which is comparable with that of PL.

2. An explanation for the shape of the forward bias current

Our early theoretical research¹⁸ has focused on the problem of finding an explanation for the shape of the forward bias current as a function of photodegradation. We have made little progress on it.

We have seen in Fig. 10 and 12, that photodegradation does not affect the final current as much as it prolongs the rise of the forward bias current. At present we can only speculate that this strange result comes about because the recombination in steady state is controlled by tail states, but the transient current is controlled by the density and capture rate of deep defect centers, that must be filled in order for the quasi-Fermi level to rise. We plan to calculate these results more carefully; but at present we only have a naive phenomenological model. What Fig. 12a and 12b show is that the forward current-rise time product, $I_f t_r$, increases with photodegradation. The quantity $I_f t_r$ can be estimated from the following phenomenological argument. From Eq. (5) and the relation of $t_r = \tau (1 + n_t/n) \approx \tau (n_t/n)$ where n_t and n are the density of trapped and free carries, respectively, one has

$$I_f t_r = \frac{CV}{t_0} \frac{\tau}{t_0} \tau \frac{n_t}{n}. \quad (6)$$

Now, because $\tau = (N_r b)^{-1}$, by assuming the density of the recombination centers, N_r , is approximately the same as the injected charge concentration, $\frac{CV}{t_0} \frac{\tau}{t_0}$, one can write

$$\tau = \frac{1}{b \frac{CV}{eL} \frac{\tau}{t_0}}, \quad (7a)$$

$$\text{and } \tau^2 = \frac{eL t_0}{bCV} \quad (7b)$$

Finally, by inserting Eq. (7b) into Eq. (6), one has

$$I_f t_r = \frac{eL}{b t_0} \frac{n_t}{n}. \quad (8)$$

The gain-band-width product is $G\Delta B = (\tau/t_0)(1/\tau) = 1/t_0$, and when $VC \geq enL$, t_0 is equal to the dielectric relaxation time, $\tau_{rel} = (\kappa/4\pi\sigma)10^{-12}$. The I_{fr} product in Eq. (8) is somewhat like the gain-band-width product in photoconductors. If I_{fr} is to increase upon photodegradation, either b or t_0 must decrease, or n_t/n increase. It is not likely that t_0 decreases because this would imply an increase in band mobility contrary to experiments. Consequently, either n_t/n increases or the recombination rate constant, b , for photogenerated defects is smaller than those for thermal defects. This requires further study.

Now, the defect-relaxation^{5,6,10-12} seems to be involved in light-soaking effects. The above phenomenological model requires substantiation before it can be accepted. Nevertheless, it seems plausible to suppose that photogenerated defects are formed in regions of high strain or local potential energy and therefore might have a small recombination rate constant because of the barriers still present after formation of the defect.

3. A Microscopic Model for Radiative Recombination^{2,19,20}

We have now succeeded in putting forth a microscopic model for low-temperature luminescence and, therefore, recombination.^{19,20} We have included the effects of the coulomb interaction and the magnitude of the localization radius on the low temperature luminescence. For small energetic disorders, the coulomb interaction produces anisotropic recombination dynamics while, for large disorder, the recombination remains isotropic. A small ($< 10^{-7}$ cm) localization radius leads to a transport-controlled recombination where the lifetime is governed by the longest jump between tail states rather than the final radiative jump between the electron and hole. Using these ideas we use Monte-Carlo methods to calculate the frequency dependence of the luminescence and show that there are two peaks, as a function of excitation density.²⁰ Our theoretical results agree well with the EL lifetime distribution data⁷ shown in Fig. 5 and 6. The lifetime of the fast process was calculated to be $\tau_f = 10^{-6}$ s for a-Si:H, independent of generation rate and material quality. The transport lifetime τ_s was shown to depend on all these parameters.

We suggest that similar physics is at the origin of high-temperature luminescence ($T > 50$ K). The model we propose is one in which two independent processes occur simultaneously, each producing its own structure in the recombination lifetime distribution. Physically, this occurs because the coulomb interaction makes the sample microscopically inhomogeneous. The transport time is approximately equal to the emission time from the quasi-Fermi level up to the transport level because most other transitions take place from shallower states. The radiative time is assisted by the coulomb interaction and takes approximately 10^{-6} s. The total lifetime is then

$$\tau = 10^{-6}s + \frac{1}{\nu_0} \exp\left(\frac{\Delta}{kT}\right) \quad (9)$$

where Δ is equal to the energy separation between the quasi-Fermi level and the transport level, and ν_0 is a rate prefactor of order 10^{12} s⁻¹.¹¹ The lifetime of this process depends on the details of the density of state as well as temperature. We suggest that the slow component in the lifetime distribution is a consequence of this process.

One measurable consequence of this model is that both τ_s and the forward bias current should share a common activation energy Δ . This is so because the current (free carrier density) is also

controlled by the separation between the electronic quasi-Fermi level and the transport level. Experimentally, the current activation energy is of order 0.2-0.25 eV in the range 150 K < T < 250 K and is smaller below 150 K (12 V bias). This is in agreement with the results in Fig. 6. A second consequence of the model is that an increase in the defect density must produce a single lifetime peak located at 10⁻⁶s because at high defect density, the only luminescence should come from those electrons initially trapped within the capture radius of a hole. This is in agreement with the results in Fig. 9b for 0.4 μm p-i-n cells.

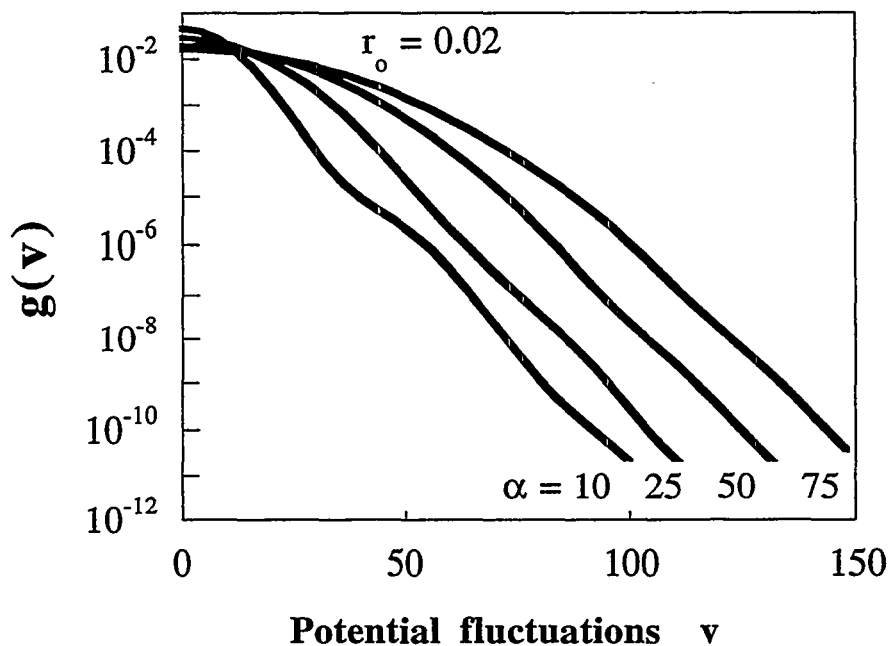


Fig. 20 Distribution of potential fluctuation v due to a dilute density of charges

Figure 20 shows typical results of our analytic calculations on the density of states due to random charges.⁶ The distribution is gaussian for small potential fluctuation v (low energies) and exponential for large values. The logarithmic slope in the exponential region depends primarily on the dielectric constant and the size of the localized site. With increased system size α , the width of the gaussian increases, but the characteristic energy of the exponential remains unchanged.

We have also studied the recombination kinetics in order to distinguish between geminate and non-geminate recombination. Our calculated results show that non-geminate recombination is faster than geminate, contrary to prior misconceptions, because the recombination pathway to a non-geminate partner is shorter at high excitation density than to its geminate pair.

4. H-diffusion Including Deep Trap Levels²¹

Because H diffusion plays an important role in the metastable effect of a-Si:H, we have considered the problem of deuterium diffusion at early times including traps.²¹ One can see in Fig. 21 an exponential tail as a function of the D position. From the slope of the tail, one can estimate the mean distance an atom moves normal to the surface and the number of the jumps it makes before deep trapping. We estimate the distance to be of order 200 Å and the number of jumps to be 10⁴.

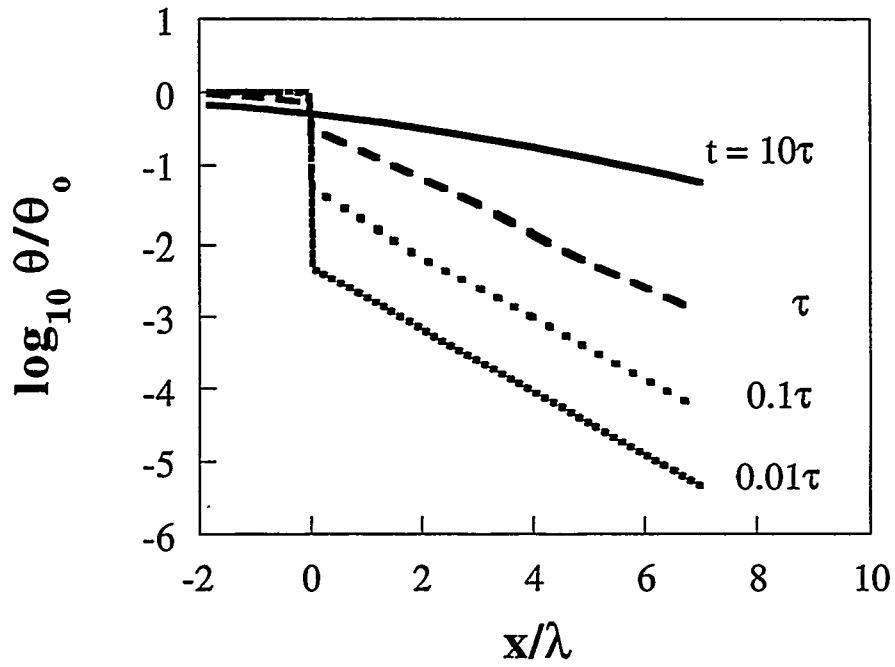


Fig. 21 D diffusion profile for four different times after the onset of diffusion. Position, x , is scaled by the mean atomic displacement between trapping events λ . Time, t , is scaled by the detrapping time τ . Tracer concentration, θ , is scaled by the initial tracer density θ_0 .

REFERENCES

1. "Electroluminescence and Forward Bias Current in p-i-n and p-b-i-n a-Si:H Solar Cells," Keda Wang, Marvin Silver, and Daxing Han, *J. Appl. Phys.* **73**, 4567 (1993).
2. "Recombination and Metastability in Amorphous Silicon and Silicon Germanium Alloys," NREL Annual Subcontract Report (1 February 1992 - 31 January 1993), Marvin Silver, UNC-CH.
3. "Recombination and Metastability in Amorphous Silicon and Silicon Germanium Alloys," NREL Annual Subcontract Report (1 February 1993 - 31 December 1993), UNC-CH.
4. "Thickness Dependence of Electroluminescence in a-Si:H p-i-n Devices," Keda Wang, Daxing Han, and Marvin Silver, "Amorphous Silicon Technology," *MRS Proc.* **297**, (1993) 857.
5. "Optical Bias Effect on Electron-Drift Measurements and Defect Relaxation in a-Si:H," Daxing Han, Douglas C. Mecher, E. Schiff, and M. Silver, *Phys. Rev.* **B48**, 8658 (1993).
6. "Photocurrent Drift and Recombination in a-Si:H: the Vital Importance of Defect Relaxation," E. A. Schiff, H. M. Branz, D. X. Han, D. C. Melcher, and M. Silver, *J. Non-Cryst. Solid* **164-166**, 331-334 (1993).
7. "Time-Resolved Transient Electroluminescence in a-Si:H," Keda Wang, Daxing Han, Mathieu Kemp, and Marvin Silver, *Appl. Phys. Lett.* **62**, 157 (1993).
8. "The Effect of Photodegradation on Electroluminescence in a-Si:H Devices," Keda Wang, Daxing Han, and Marvin Silver, **164-166**, 595-598 (1993).
9. "Light Induced Metastable Defects in a-Si:H Studied by Transient Space Charge Perturbed Currents," Daxing Han, Keda Wang, and M. Silver, *J. Non-Cryst. Sol.* **137/138**, 267(1991).
10. "Transient Forward Bias Current in a-Si:H p-i-n Devices," Daxing Han, Keda Wang, and M. Silver, **164-166**, 339-342 (1993).
11. "What Electroluminescence and Transient Space Charge Limited Currents Tell Us about Steabler-Wronski Effects," Keda Wang, Daxing Han, and Marvin Silver, "Amorphous Silicon Materials and Solar Cells," *AIP Conference Proc.* **234**, ed. Byron L. Stafford, (New York, 1991), 162.
12. "Reverse Recovery and Decay of Stored Excess Carriers in a-Si:H p-i-n Diode," Daxing Han, Keda Wang, and M. Silver, "Amorphous Silicon Technology," *MRS Proc.* **258**, 837 (1992).
13. "Effect of Photo-Degradation on Transient and Steady State Forward Bias Characteristics of a-Si:H p-i-n Diode," R. Amokrane, R. Vanderhaghen, and M. Silver, "Amorphous Silicon Technology," *MRS Proc.* **258**, 467 (1992).
14. "Effect of Light-Induced Degradation on Photoconductive Gain in a-Si:H n-i-p Devices," R. Vanderhaghen, R. Amokrane, D. X. Han, and M. Silver, **164-166**, 599-602 (1993).
15. "Temperature and Current Dependence of Electroluminescence in a-Si:H," K. D. Wang, D. X. Han, M. E. Zvanut, and M. Silver, *Phil. Mag.* **B63**, 175 (1991).
16. "Electroluminescence Studies of Recombination in Hydrogenated Amorphous Silicon p-i-n Devices," Keda Wang, Daxing Han, Marvin Silver, and Howard Branz, *Solar Cells*, **30**, 219 (1991).
17. "Electroluminescence: A Study of Non-Geminate Radiative and Non-Radiative Bulk Recombination," Keda Wang, Daxing Han, Mathieu Kemp, and Marvin Silver, *J. Non-Cryst. Sol.* **137/138**, 599 (1991).
18. "Recombination and Metastability in Amorphous Silicon and Silicon Germanium Alloys," NREL Annual Subcontract Report (1 February 1991 - 31 January 1992), Marvin Silver, UNC-CH.
19. "The Puzzle Surrounding Luminescence Models," M. Kemp and M. Silver, *J. Non-Cryst. Sol.* **141**, 88 (1992).
20. "A Monte Carlo Investigation of Low-Temperature Geminate Pair Recombination Dynamics in Amorphous Semiconductors," M. Kemp and M. Silver, *Phil. Mag. Lett.* **66**, 169 (1992).
21. "Analytic Solution of Trap-Controlled Tracer Diffusion in Amorphous Solids," M. Kemp and H. Branz, *Phys. Rev. B* **47**, 7061 (1993).
22. "Metastability in Hydrogenated Amorphous Silicon: The Adler Model Revised," H. M. Branz, R. S. Crandall, and M. Silver, *AIP Conf. Proc.* **234**, Amorphous Silicon Materials and Solar Cells," (AIP, New York, 1991) 29.

REPORT DOCUMENTATION PAGE

Form Approved
OMB NO. 0704-0188

Public reporting burden for this collection of information is estimated to average 1 hour per response, including the time for reviewing instructions, searching existing data sources, gathering and maintaining the data needed, and completing and reviewing the collection of information. Send comments regarding this burden estimate or any other aspect of this collection of information, including suggestions for reducing this burden, to Washington Headquarters Services, Directorate for Information Operations and Reports, 1215 Jefferson Davis Highway, Suite 1204, Arlington, VA 22202-4302, and to the Office of Management and Budget, Paperwork Reduction Project (0704-0188), Washington, DC 20503.

1. AGENCY USE ONLY (Leave blank)	2. REPORT DATE July 1994	3. REPORT TYPE AND DATES COVERED Final Subcontract Report—1 February 1991 - 31 January 1994	
4. TITLE AND SUBTITLE Recombination and Metastability in Amorphous Silicon and Silicon-Germanium Alloys		5. FUNDING NUMBERS C: XG-1-10063-5 TA: PV431101	
6. AUTHOR(S) M. Silver, D.X. Han, K.D. Wang, M. Kemp		7. PERFORMING ORGANIZATION NAME(S) AND ADDRESS(ES) University of North Carolina Chapel Hill, North Carolina	
9. SPONSORING/MONITORING AGENCY NAME(S) AND ADDRESS(ES) National Renewable Energy Laboratory 1617 Cole Blvd. Golden, CO 80401-3393		8. PERFORMING ORGANIZATION REPORT NUMBER 10. SPONSORING/MONITORING AGENCY REPORT NUMBER TP-451-6491 DE94011837	
11. SUPPLEMENTARY NOTES NREL Technical Monitor: H. M. Branz			
12a. DISTRIBUTION/AVAILABILITY STATEMENT		12b. DISTRIBUTION CODE UC-271	
13. ABSTRACT (<i>Maximum 200 words</i>) Electroluminescence-spectra- and transient-current measurements were taken before and after light-soaking a-Si:H p-i-n structures. For the first time, we were able to distinguish between bulk- and junction-controlled recombination. We found that in buffered p-b-i-n structures, the main-band luminescence was more pronounced than that in simple p-i-n structures. The enhancement of the main-band luminescence relates with an increase of the open-circuit voltage. This is evidence that the recombination takes place near the p-i interface, and the quality of the p-i interface is very important in solar cell performance. We also found that for thick p-i-n cells ($\geq 2 \mu\text{m}$), the luminescence contains more high-energy photons (1.1–1.2 eV) than does that for thin cells. Furthermore, the high-energy recombination is more efficient in creating metastable defects than is the low-energy recombination. Consequently, the thinner the i-layer, the less the light-induced effects. The results of repetition rate and reverse bias effects on forward-bias current imply that the junctions recover faster than the bulk when subjected to excess carriers caused by the bias. By including the coulomb interaction, we made progress on a microscopic model for radiative recombination.			
14. SUBJECT TERMS recombination ; metastability ; amorphous silicon ; silicon-germanium ; alloys ; photovoltaics ; solar cells		15. NUMBER OF PAGES 37 16. PRICE CODE A03	
17. SECURITY CLASSIFICATION OF REPORT Unclassified	18. SECURITY CLASSIFICATION OF THIS PAGE Unclassified	19. SECURITY CLASSIFICATION OF ABSTRACT Unclassified	20. LIMITATION OF ABSTRACT UL